ESSA RESEARCH LABORATORIES
Air Resources Laboratories
Silver Spring, Maryland
December 1968

Atmospheric Transport and Diffusion in the Planetary Boundary Layer

Technical Memorandum ERLTM-ARL 9

U.S. DEPARTMENT OF COMMERCE / ENVIRONMENTAL SCIENCE SERVICES ADMINISTRATION

U.S. DEPARTMENT OF COMMERCE
ENVIRONMENTAL SCIENCE SERVICES ADMINISTRATION
RESEARCH LABORATORIES

ESSA Research Laboratories Technical Memorandum -ARL 9

ATMOSPHERIC TRANSPORT AND DIFFUSION IN THE PLANETARY BOUNDARY LAYER

I. Van der Hoven, Editor

Contributors

J. K. Angell
A. B. Bernstein
D. L. Bjorem
C. R. Dickson
G. A. Herbert
G. E. Start
D. H. Slade
L. L. Wendell
F. E. White

Semiannual Research Program Review
January - June 1968
for the Division of Reactor Development and Technology
U. S. Atomic Energy Commission

AIR RESOURCES LABORATORIES
TECHNICAL MEMORANDUM NO. 9

SILVER SPRING, MARYLAND 20910
DECEMBER 1968

Preface

In accordance with the letter of agreement of July 10, 1967, with the U. S. Atomic Energy Commission, Division of Reactor Development and Technology, Environmental and Sanitary Engineering Branch, the Air Resources Laboratories have continued their study of atmospheric transport and diffusion in the planetary boundary layer, micrometeorology, diffusion climatology, and the application of this work to the disposal of radioactive waste gases into the atmosphere. The research is technically administered and supervised through the Air Resources Environmental Laboratory of the Air Resources Laboratories. The work is performed at the Air Resources Laboratories Headquarters in Silver Spring, Maryland, and at the Air Resources Idaho Falls Laboratory, National Reactor Testing Station, Idaho. Any inquiry on the research being performed should be directed to the editor, Isaac Van der Hoven, Chief, Air Resources Environmental Laboratory, Air Resources Laboratories, Environmental Science Services Administration, 8060 13th Street, Silver Spring, Maryland 20910.

Table of Contents

ATMOSPHERIC TRANSPORT AND DIFFUSION IN THE PLANETARY BOUNDARY LAYER

AIR RESOURCES LABORATORIES SEMIANNUAL RESEARCH PROGRAM REVIEW
FOR THE ENVIRONMENTAL AND SANITARY ENGINEERING BRANCH
DIVISION OF REACTOR DEVELOPMENT AND TECHNOLOGY
U. S. ATOMIC ENERGY COMMISSION

JANUARY - JUNE 1968

1.0 RESEARCH AT AIR RESOURCES LABORATORIES HEADQUARTERS, SILVER SPRING, MD.

1.1 Low Altitude Constant Volume Balloon (Tetroon) Trajectories

(This project is a joint effort by personnel of the Air Resources Laboratories in Silver Spring, Maryland, and field offices. Support is provided jointly by the Atomic Energy Commission and the Public Health Service.)

A tetroon experiment was carried out at Jackass Flats on the Nevada Test Site during May and June. Forty tetroons, ballasted to float at 1000 ft, were flown by the 1500-ft BREN tower, with the primary purpose of comparing periods of vertical oscillation in Eulerian and Lagrangian frames of reference. The tetroons were equipped with transponders and were positioned at 30-s intervals by one or two M-33 radars. Eighty hours of tetroon track were obtained. During the time of the flights, bivane data were obtained at heights near 500 and 1500 ft on the BREN tower, together with temperature data at these and several other levels. This experiment will also provide additional information on tetroon vertical periodicities as a function of lapse rate, as well as information on air flow over mountains. Finally, the considerable time when two radars were tracking the same tetroon should provide interesting data concerning the accuracy and representativeness of M-33 tracks on the tetroon-transponder system. The rather large data-reduction task associated with this experiment is now underway.

A computer program has been compiled that determines, theoretically, the relation between air parcel and tetroon oscillation in the vertical. The program includes the effects of dynamic buoyancy as well as the more conventional buoyancy and drag forces. The program permits one easily to note the effect of varying drag force, period and amplitude, etc. Preliminary trials, if we assume a sinusoidal air parcel trajectory, suggest that the tetroon trajectory closely follows the air parcel trajectory vertically, with differences in amplitude of less than 10 percent. The program will be applied to more realistic air parcel trajectories by superimposing sinusoidal oscillations of different period.

1.2 Survey of Radiological Safety Analysis Computer Programs

(This project is a joint effort by personnel of the ESSA Air Resources Environmental Laboratory and the AEC Division of Reactor Development and Technology.)

A number of computer codes to estimate radiological doses from a continuous plume of radioactive gases have been developed and used by nuclear laboratories, testing facilities, and reactor manufacturers. These codes make possible the computation of whole body gamma ray doses and inhalation thyroid doses from the passing cloud. Required input to the code includes the reactor size, the duration of full power operation, the fission product release fractions to the containment building atmosphere, the release rate and height to the outside atmosphere, the three-dimensional cloud concentration distribution, and the conversion factors from cloud concentration to radiological dose.

Increasingly, these codes are being used in nuclear reactor safety analyses. Review of these analyses has indicated some inconsistencies when spot checks of downwind doses, especially cloud gamma doses, were hand-computed for cases that should have yielded similar results. Since the sophistication and complexity of current computer codes make it difficult to pin-point trouble spots, a standardized reactor accidental effluent release problem was prepared and sent to a number of private and governmental organizations for a computer code analysis.

The standard problem specified the following: 1) 1000-MW thermal reactor operating for 300 days, 2) release to the containment building atmosphere of 100 percent of the noble gases, 25 percent of the halogens, and 1 percent of the solids, 3) release rates to the outside air, of all the available (airborne in containment building) radioactivity in 1 hr and 1 percent in 24 hr, 4) releases from ground level and from a stack height of 100 m with no further effective stack rise, and 5) atmospheric diffusion types defined by Pasquill category "F" with a wind speed of 1 m/s and category "C" with a wind speed of 4 m/s. We reasoned that the standardized problem would point out source term and computational differences. The agreement (or lack thereof) among computations, of course, is not proof of the accuracy (or inaccuracy) of the computer code used, since there are no absolute standards for judging the accuracy of dose computations, but we hoped through these code comparisons to identify the obvious reasons for disagreement. Of the 10 participants (including the AEC Division of Reactor Licensing, Environmental and Radiation Safety Technology Branch) six made computations for all conditions, namely, ground and 100 m release height, stable and neutral meteorological conditions, 1 and 24-hr release times, and whole body gamma and thyroid inhalation doses. The participants are identified by the letters A through J in the comparisons that follow.

Although the reactorsize and operating history were specified in the problem, it was left to the particpants to select through their codes the important isotopes, the fission product chains, and the appropriate treatment of isotope buildup and decay. Table 1 lists the information, supplied by the

Table 1. Radioactive Inventory (Curies) Available for Release to Atmosphere at Initiation of Excurison

Participant	A	B	C	D*	F	I*	J
Noble Gases		5.38×10^8	3.92×10^8	1.93×10^8	4.23×10^8	1.84×10^8	5.05×10^8
Halogens		1.08×10^8	1.21×10^8	0.59×10^8	0.97×10^8	0.73×10^8	0.63×10^8
Solids		0.36×10^8	1.19×10^8	0.14×10^8	0.35×10^8	0.14×10^8	0.25×10^8
TOTAL	6.82×10^8	6.82×10^8	6.32×10^8	2.66×10^8	5.55×10^8	2.71×10^8	5.93×10^8

*Data supplied in Mev/s and Mev/disintegration but listed as curies by use of the conversion factor 1 curie = 3.7×10^{10} disintegration/s.

participants, on the radioactive inventory available for release to the atmosphere at the initiation of the excursion. The inventory, in curies, includes 100, 25, and 1 percent release fraction to the containment building atmosphere, respectively, for noble gases, halogens, and solids. Differences by a factor of two are evident in the initial inventories. To show the effect of radioactive decay and the production of isotopic daughter products, the inventory for the first 24 hr is given in figure 1 for those participants who were able to supply the information. The maximum difference here is about a factor of 1.8.

The primary parameters in the thyroid inhalation dose calculations are (1) halogens released to the outside atmosphere, (2) downwind atmospheric diffusion rate, (3) human breathing rate, and (4) thyroid uptake fraction. Essentially, these parameters behave as constants with downwind distance, except for atmospheric diffusion, which was specified in the test problem as shown by Hilsmeier and Gifford (1962). Examples of the results of the thyroid dose calculations are shown in figures 2 through 5, with each participant labeled as indicated previously. Except for curve H, agreement is within a factor of 1.5. The only known differences in parameters are the halogen source terms shown in table 1 and the use of a lower breathing rate (2.3×10^{-4} as against 3.5×10^{-4} m^3/s) by participants B and E. From the Hilsmeier and Gifford (1962) curves for a 100-m stack height, one would expect the type C and F elevated releases dose peaks at distances of 1000 m and 15,000 m, respectively. This is consistent with the results shown in figures 4 and 5.

Of all radiological dose calculations, the computation of whole body gamma dose from a passing finite cloud is the most complex. A simplified procedure is to assume that the dose recipient is immersed in the center of a semi-infinite cloud. The computation then becomes similar to the thyroid inhalation dose, namely, the product of the downwind centerline ground concentration and a constant factor. Participants B, F, G, I, and J used this simplifying assumption. For the ground release this would be a conservative approach, especially at close-in distances. For the elevated release it should result in a nonconservative dose computation, especially between the point of release and the point of maximum ground level concentration. The more complex computation consists of determining the gamma dose contribution of each element of the finite cloud, whose dimensions and concentration profiles are fully described. This was the procedure followed by the remainder of the participants, and examples of the results are shown in figures 6 through 9. For the ground releases (figs. 6 and 7) there are obvious orders of magnitude differences among the curves. The high values for curves B, F, G, I, and J at close-in distances in figure 6 and for curves B, G, I, and J in figure 7 are probably caused by the semi-infinite cloud assumption, but there is no obvious explanation for the remainder of the differences in the ground releases. Agreement among the elevated releases is quite good (figs. 8 and 9), except for curve B, which at close-in distance for inversion conditions (fig. 9) is lower, by a factor of 5, than the main grouping. Participant B indicated that for the elevated release the semi-infinite cloud computation was manually corrected for finite size by use of an approximate method.

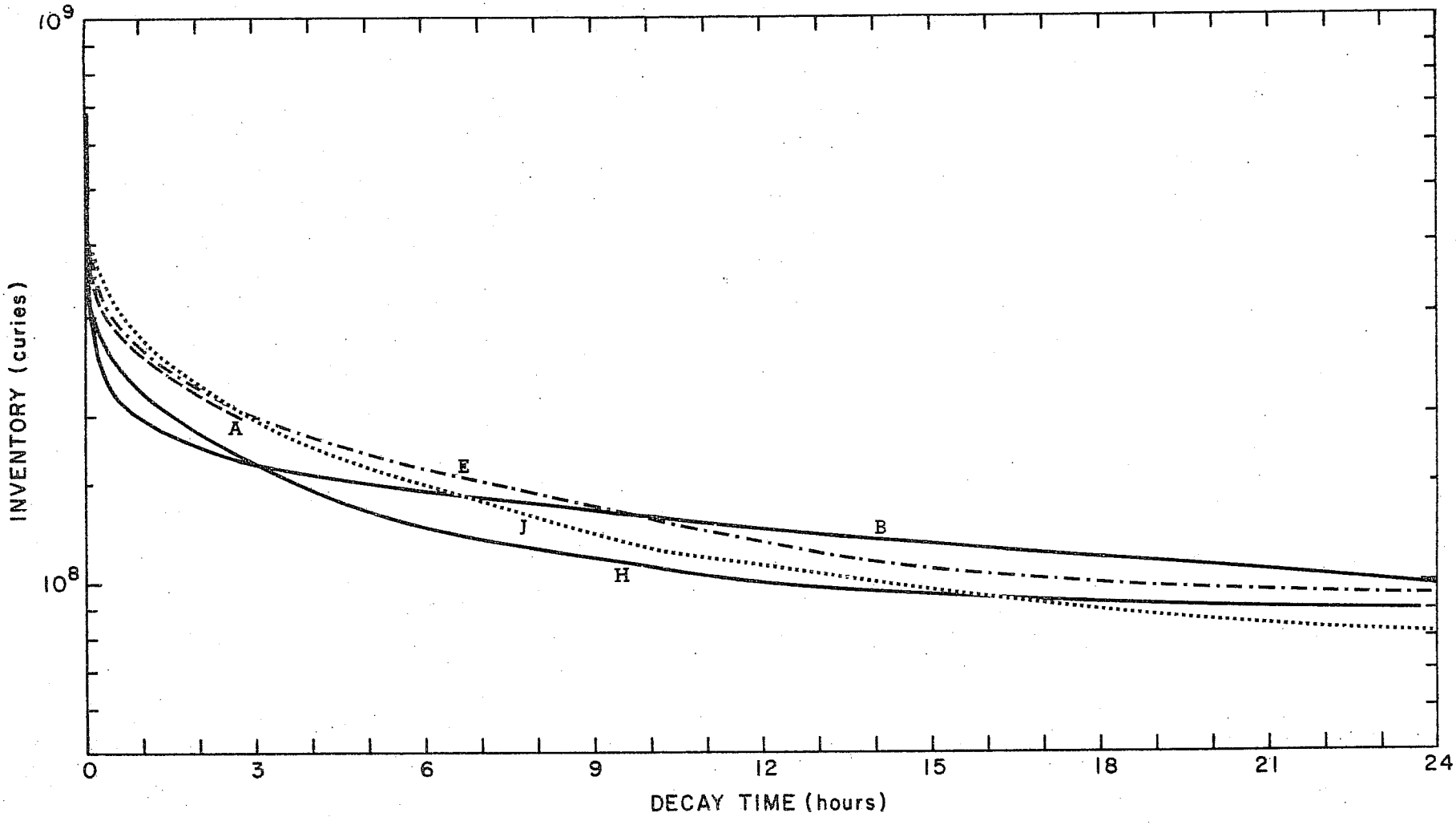

Figure 1. Radioactive inventory following postulated release from a 1000-MW thermal reactor operating for 300 days.

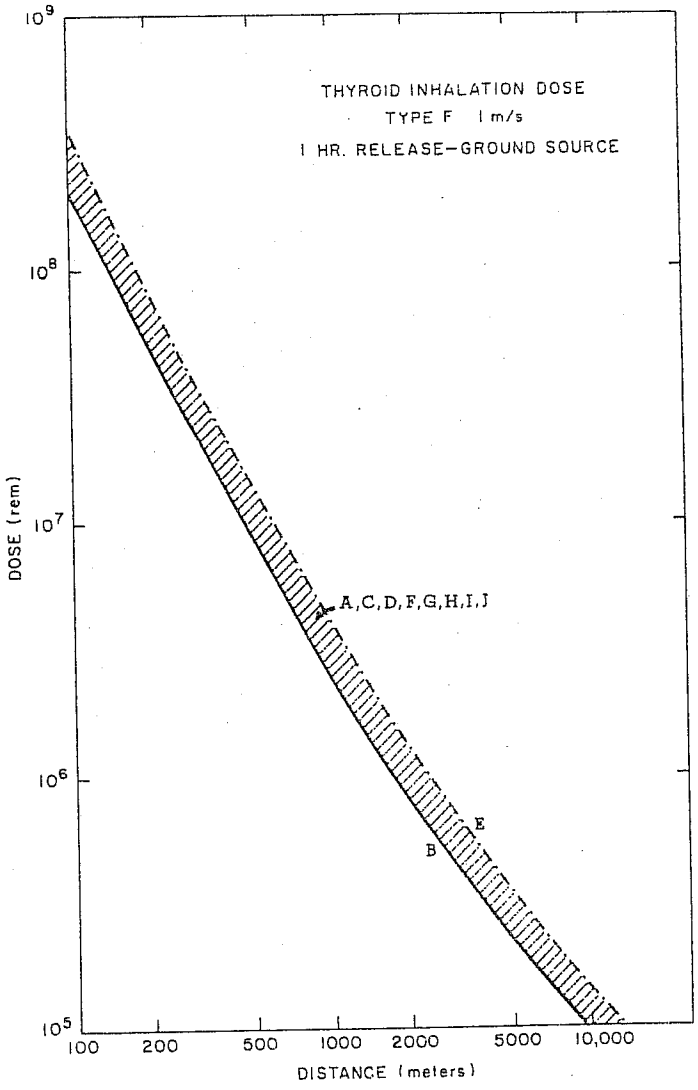

Figure 2. Thyroid inhalation dose for 1-hr reactor release at ground level under inversion conditions.

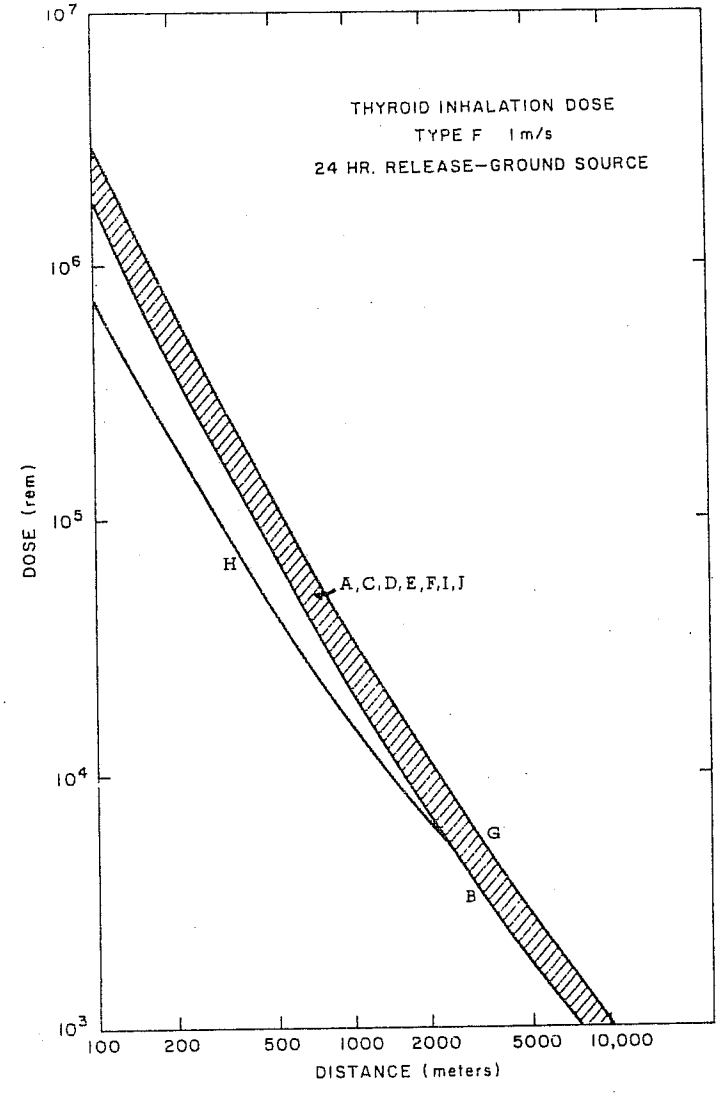

Figure 3. Thyroid inhalation dose for 24-hr reactor release at ground level under inversion conditions.

B-79145

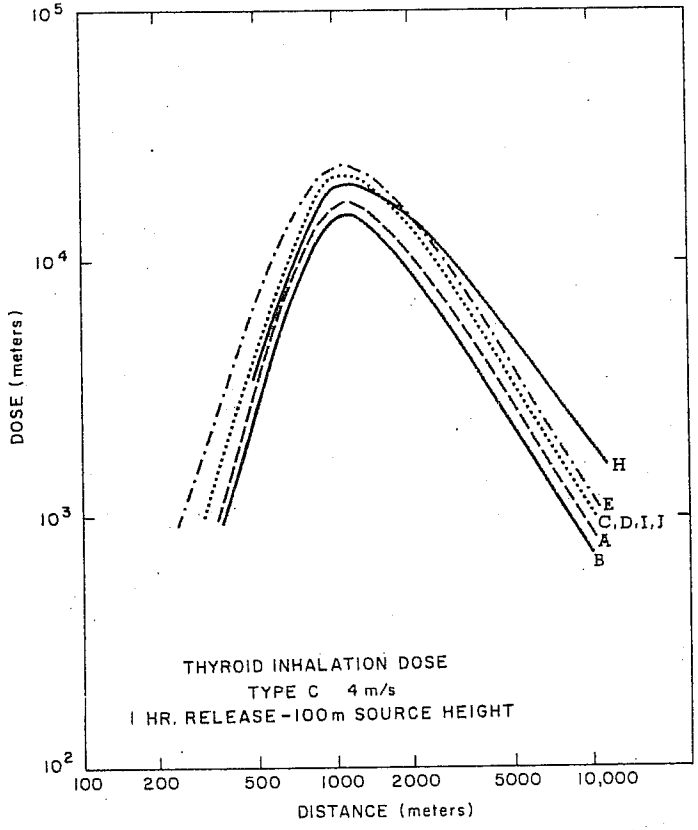

Figure 4. Thyroid inhalation dose for 1-hr reactor release at 100 m under neutral conditions.

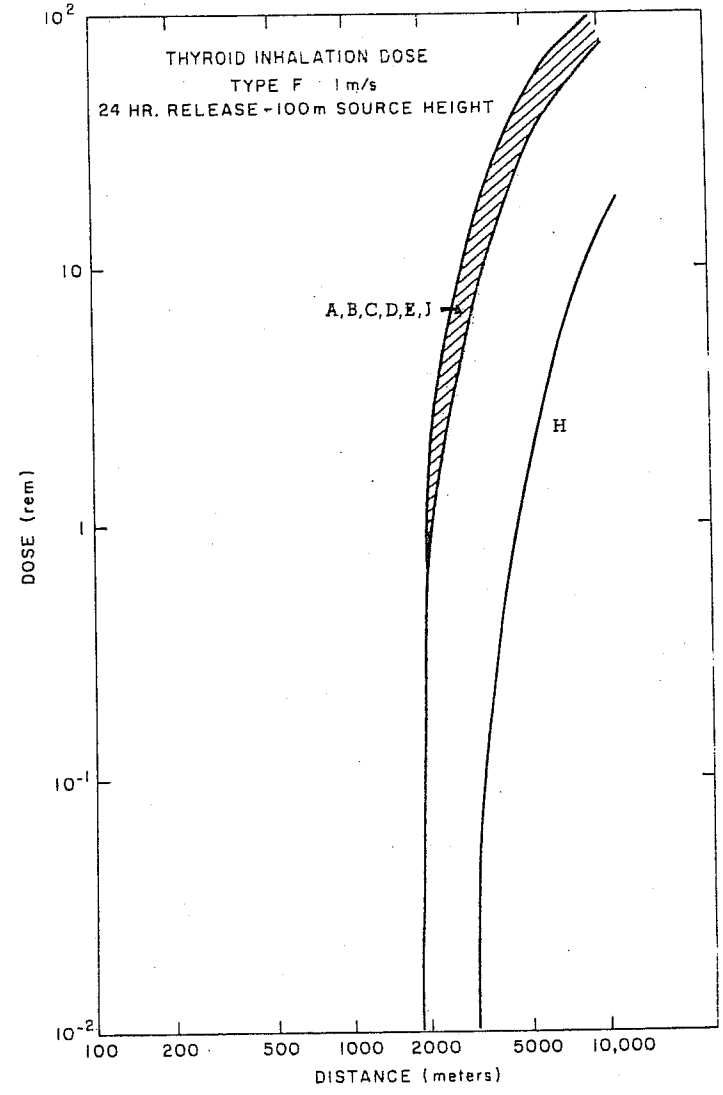

Figure 5. Thyroid inhalation dose for 24-hr reactor release at 100 m under inversion conditions.

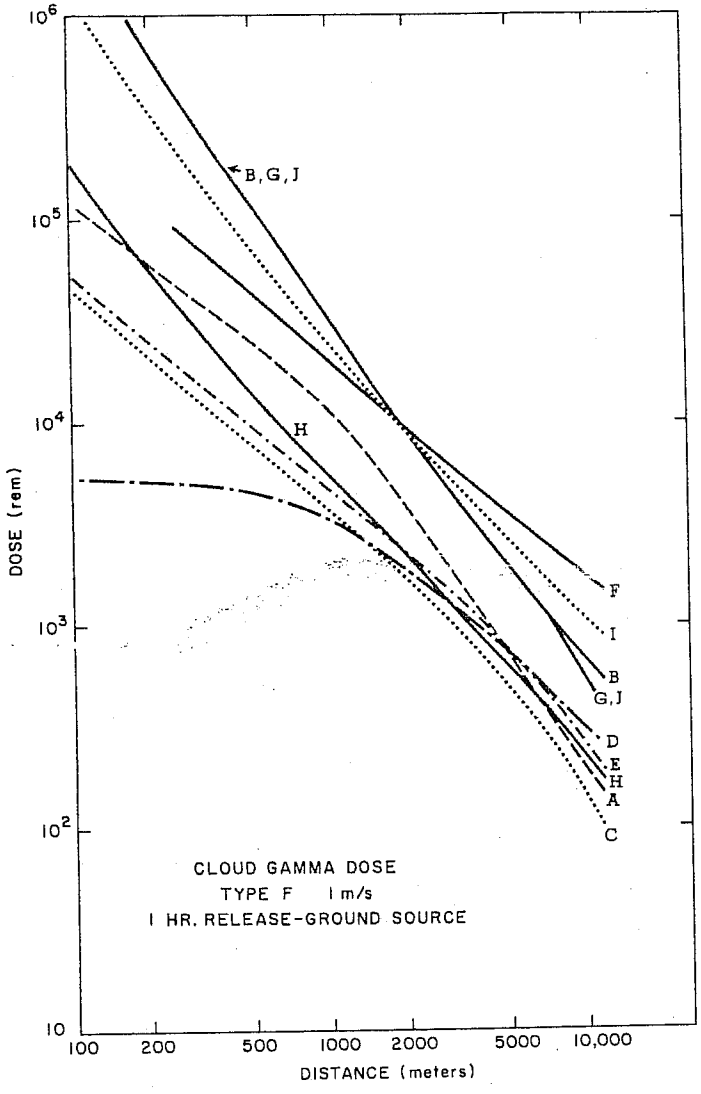

Figure 6. Cloud gamma dose for 1-hr reactor release at ground level under inversion conditions.

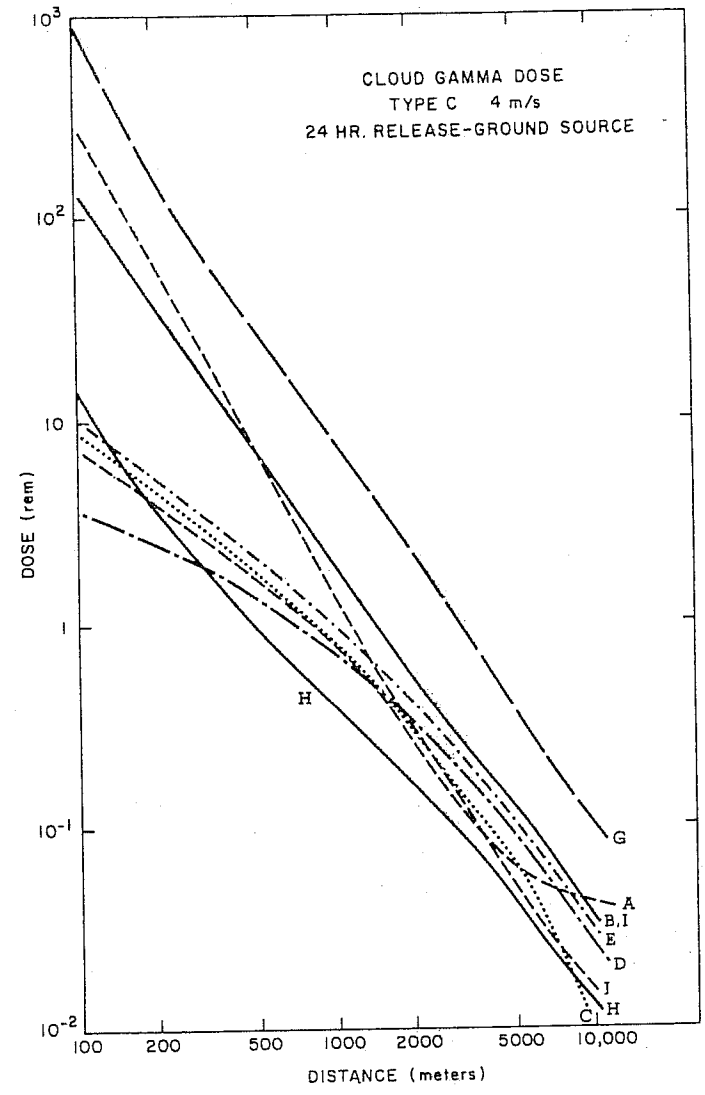

Figure 7. Cloud gamma dose for 24-hr reactor release at ground level under neutral conditions.

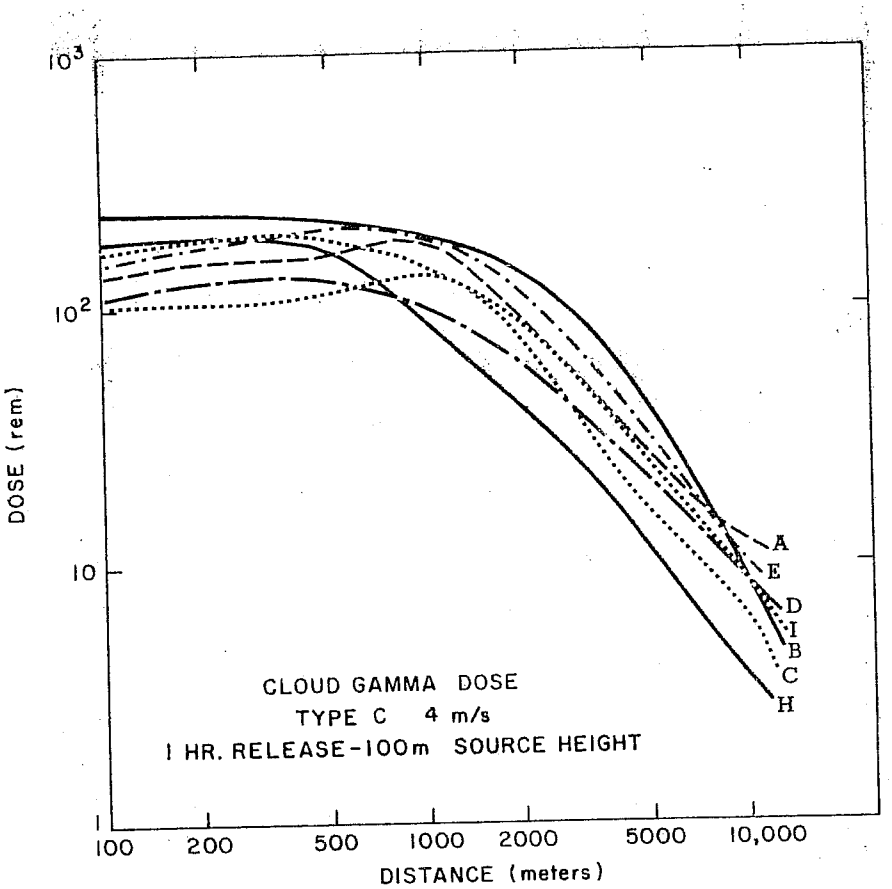

Figure 8. Cloud gamma dose for 1-hr reactor release at 100 m under neutral conditions.

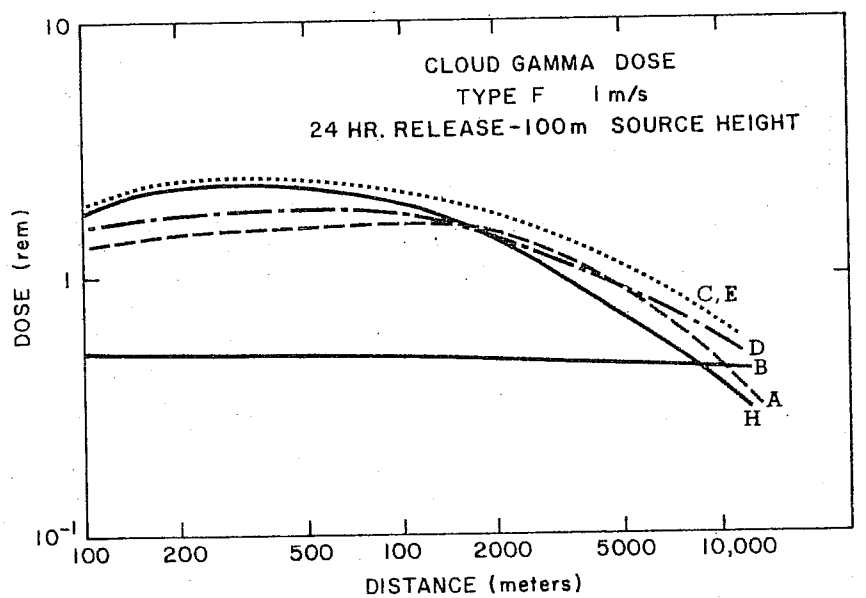

Figure 9. Cloud gamma dose for 24-hr reactor release at 100 m under inversion conditions.

B-79142

We concluded from the survey that dose calculations in which the meteorology was standardized were in reasonable agreement (factor of about 1.5) for the thyroid inhalation dose, but that the whole body gamma dose calculations disagreed considerably, especially for ground releases within a downwind distance of 1000 m. It is not clear at this point to what the difference can be attributed, nor is it possible, in an absolute sense, to determine which computation is the most accurate. Two courses of action would seem necessary: (1) field studies to measure the relationship between radioactive cloud concentration distribution and dose measurements and (2) a comprehensive study of each of the cloud gamma computer codes in order to determine the reason for computational differences. The goal would be a standardization of the procedure to yield the most accurate dose computations possible.

1.3 Boundary Layer Turbulence

The necessary reprogramming made by the change in system-processor on the CDC-6600 at Suitland forced an evaluation of all codes now in use. This seemed to be a good time to change the basic spectrum analysis routine. The slower program based on the traditional lag-correlation method (Blackman and Tukey, 1958) was replaced by a fast-Fourier-transform (FFT) routine based on the algorithm of Cooley and Tukey (1965). The input to this program is unchanged - a uniformly spaced series - but the preliminary processing is different from before. Two steps are now required: tapering the ends and shifting to a zero mean. The mean and variance of the series are computed, and the mean value is subtracted from each data point. Then the split cosine-bell taper suggested by Bingham, Godfey, and Tukey (1967) is applied so that 10 percent of the record of each end is modified. This procedure corresponds to applying a hanning window to the periodogram. Further, a zero-fill is used to extend the series to the next larger 2^n sample limit. The mean is removed, and variance of the tapered data is also computed as an internal check. A bit-flipping routine written by Mr. J. Winkelman of ESSA Research Laboratories, Boulder, for a Control Data Computer was modified by Mr. M. Smith of Air Resources Laboratories for use on the CDC-6600/scope in Suitland, Md. Included in this modification was a restructuring of the input to accept paired-data series; the processing of the second series is done in the imaginary bank. It is therefore only a matter of multiplying the Fourier transforms of each series to get the cross-periodogram; the periodogram is obtained from the self-product. The area under each periodogram is computed and used to normalize each individual value. Spectral estimates are calculated by smoothing the periodogram over third-octave bands.

A typical time series was selected from the New Jersey experiment to compare the two methods of calculating the spectra. This experiment consisted of vertical-wind component measurements from an ultrasonic anemometer at a height of 2 m (1450 EDT, October 15, 1966). The split-cosine bell taper accounted for an 11 percent reduction in variance, from 0.138 m^2s^{-2} before tapering to 0.124 m^2s^{-2} afterwards. In figure 10 the normalized spectra $n\,S(n)/\overline{(w')^2}$ from the traditional, lag-correlation method and the fast-Fourier transform program are plotted together. The slight discrepancies observed at lower frequencies are caused largely by the nonuniform width frequency bands used in the lag-correlation spectrum. Because of the small

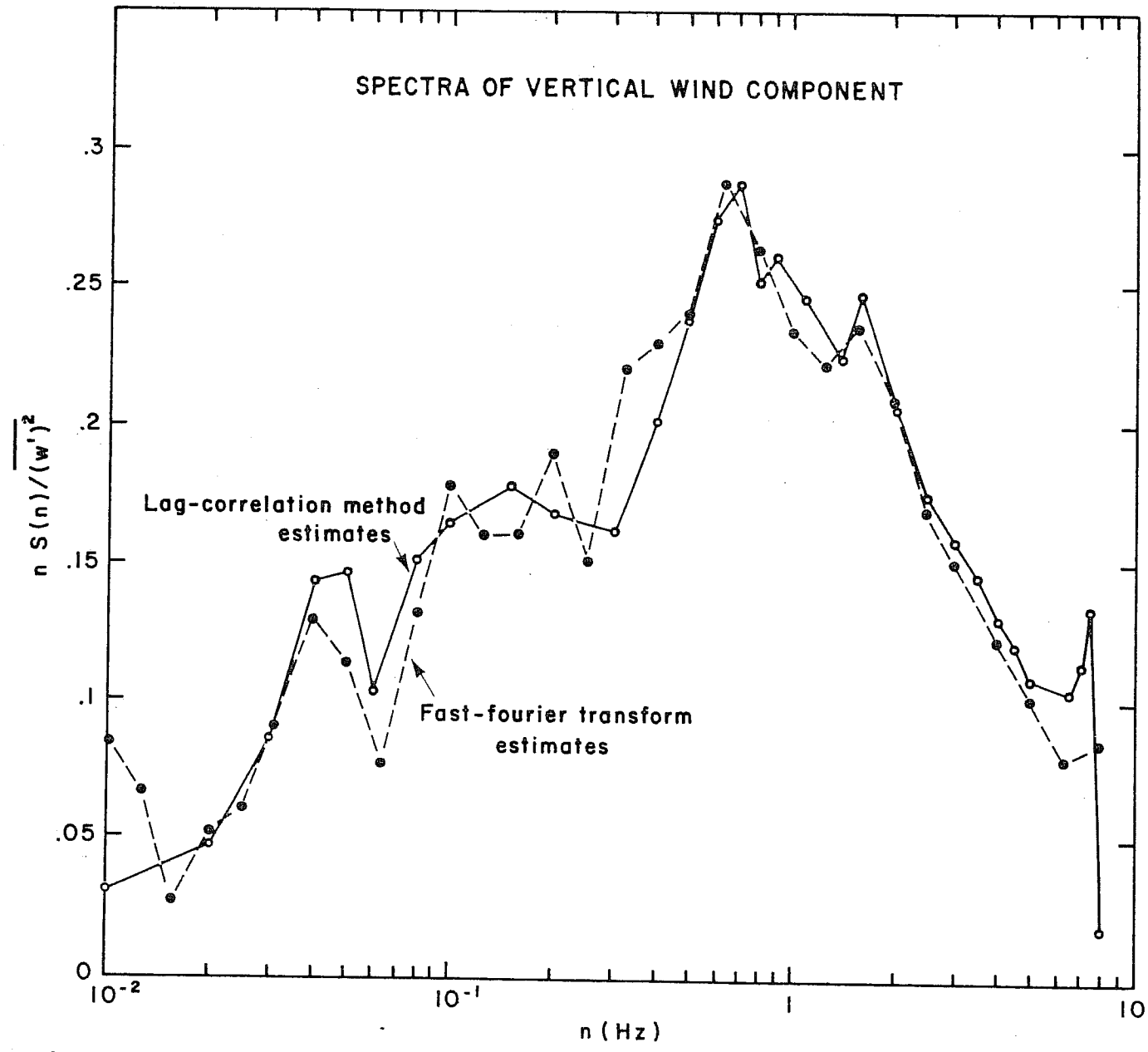

Figure 10. Comparison of normalized vertical velocity spectra as computed by lag-correlation and fast-Fourier transform methods.

resolution frequency (10^{-3} H_z) associated with the FFT method, the cross-talk between bands at high frequencies is very small and aliased energy in these bands is not transmitted to neighboring bands, as with the other estimates. The difference in computation time is most significant; the lag-correlation took approximately 10 min to compute a series pair, but the FFT routine took only 13 sec.

During a test period in the summer of 1966, the ARL infrared hygrometer, which was built to accurately measure fluctuations of absolute humidity, was subjected to a power surge, burning out a power supply. The instrument was returned to the laboratory where it was constructed, and the damaged electronics were rebuilt. Certain modifications were also made to the instrument configuration to facilitate handling in the field. The calibration and response characteristics have been checked and the instrument is now being tested, after which it will be compared with other water-vapor measuring devices (e.g., NBS Barium Chloride Cells) before being sent to NRTS, Idaho, for use in the deposition studies.

1.4 Studies of Data from Tall Towers

Three studies are in progress based on data from tall towers. The first deals with the variation of σ_v with height and was reported upon in the last semiannual report (ERLTM-ARL 5, May 1968). While the observed maximum value of σ_v at some height above the surface is typical of all the data surveyed thus far, it is not yet clear whether this is real or due to instrumental response. Study of this problem is continuing.

The second investigation deals with the vertical variation of the frequency of wind direction trace types. A typing scheme similar to Giblett's (1932) Type IV and Smith's (1950) Type D has been adopted to categorize the various trace types associated with stable atmospheric layers. To date approximately 100,000 hr of wind records have been surveyed. These data were chosen from observations made at 12 towers at levels between 30 and 444 m. Preliminary results indicate that:

(a) The daily frequency of stable trace types increases markedly with height. An example is shown in figure 11 for data to a height of 270 m from a tower in Philadelphia. At the highest level investigated (the 444-m level of the Oklahoma City, National Severe Storms Laboratory (NSSL) tower), stable trace types (labeled SR in the figure) occur for almost 60 percent of the entire year. Further, stable trace types occur for approximately 85 percent of the night hours during the year, as shown in figure 12.

(b) Stable trace types are less common over cities than over rural areas at the same height above the surface. This is illustrated in figure 13 for two 91-m towers near Washington, D. C., and for similar towers at Damascus and Waldorf, Maryland, in the rural region some 30 mi from Washington, D. C. The 50-percent frequency of smooth flow at night is found at a height of about 175 m over rural areas and is estimated to be about 300 m over cities. This suggests that mixing depths at night may be about twice as deep over cities as over rural areas.

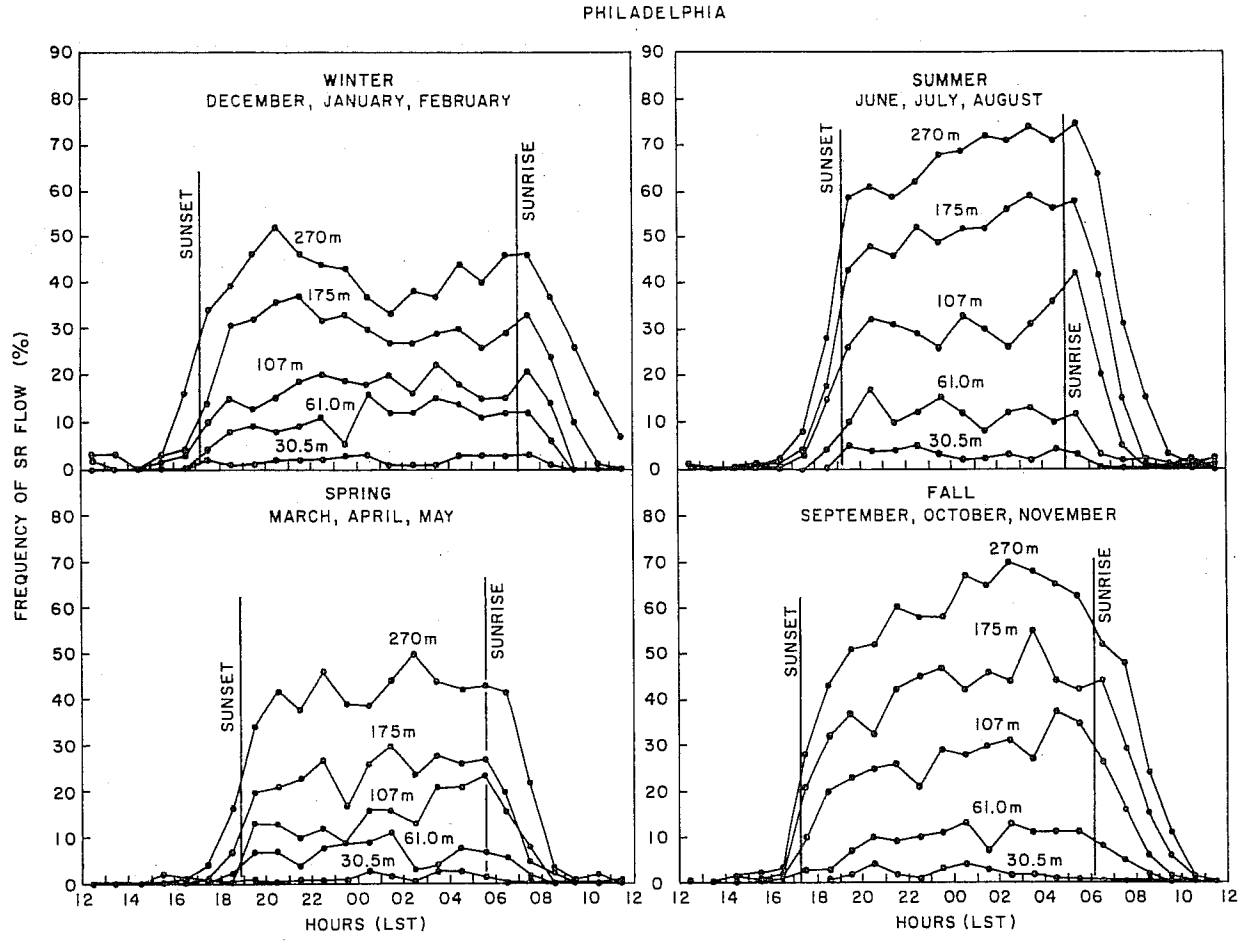

Figure 11. Frequency of stable (SR) trace types as a function of hour, height, and season.

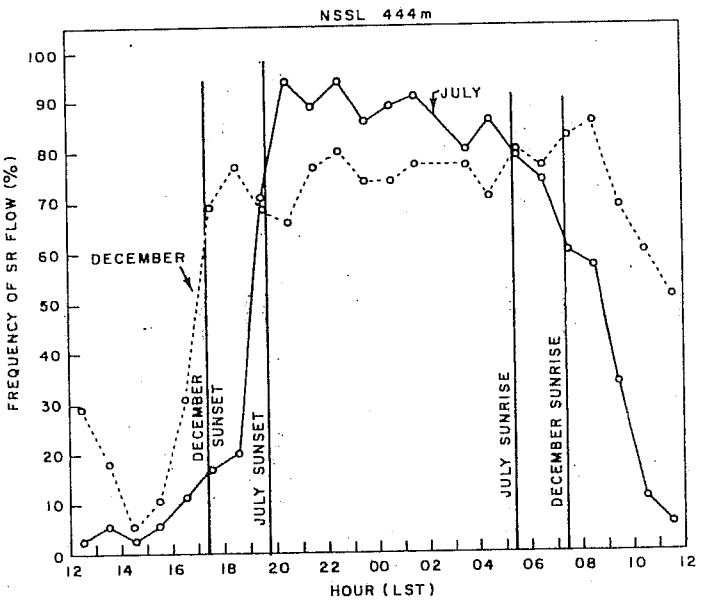

Figure 12. Hourly frequency of stable (SR) trace types at 444 m during July and December.

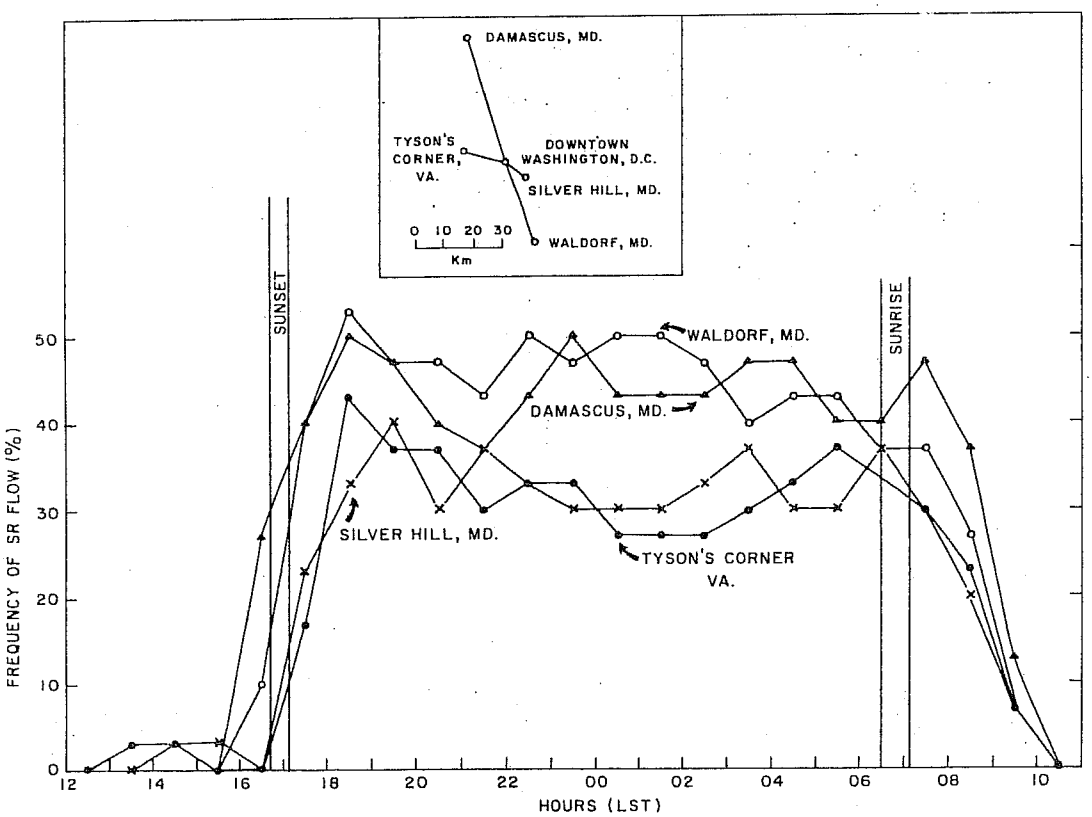

Figure 13. Hourly frequency of stable (SR) trace types over rural as compared to urban areas.

(c) As shown in figure 11, the frequency of stable trace types at a given height begins to increase shortly before sunset and remains at typical night values after sunrise. At the greater heights, these trace types may persist for 5 hr or more after sunrise and, on occasion, have been observed through an entire diurnal cycle.

(d) The 24-hr frequency of stable trace types appears to be related to the severity of air pollution at Washington, D. C. This is illustrated in figure 14 for the March and November 1966 air pollution episodes along the eastern seaboard.

(e) The turning of the mean wind direction in the planetary boundary layer as a continuous diurnal oscillation introduces a long-period dispersive mechanism which cannot be identified directly from the 1-hr trace types. However, as shown in figure 15, upper wind directions change regularly by about 3 or 4^{o}/hr on nights marked by stable trace types as opposed to no average turning during nights with turbulent flow.

The final study in progress deals with wind profiles and estimates of turbulence statistics at the very rough site of the Philadelphia (270 m) instrumented television tower. Very different turbulence and wind speed profiles are observed, depending upon whether the wind has reached the tower after passing over the Schuylkill River valley or after traversing the rough terrain in other directions. The tower data appear to be consistent with theory and with other observations.

1.5 Mixing Length Hypotheses

Most mathematical formulations of atmospheric diffusion incorporate some form of "K-theory", i.e., some assumption concerning a linear relationship between the turbulent flux of a quantity and the mean gradient of that quantity. Although there is no rigorous theoretical justification for such an assumption, the classical mixing length hypothesis introduced by Prandtl suggests a model in which turbulent mixing takes place with just such a linear relationship. However, there are numerous instances, both in the laboratory and in the atmosphere, in which the Prandtl model breaks down.

The Prandtl model is a purely kinematic model, in which, although the mixing is claimed to be due to the motion of air particles, no account is taken of the forces responsible for that motion. It specifies a mixing mechanism in which a particle representative of its environment suddenly acquires an anomalous motion without changing any of its properties, and just as suddenly loses this motion and comes into equilibrium with its new environment. This model assumes that, on the scale of this anomalous motion, the property being transferred is, in the mean, linearly distributed in space. Since the assumptions of a discrete mixing mechanism and a linear spatial distribution are known to be unrealistic, it is of interest to see what happens if the underlying kinematic description is retained but the other two features discarded. It turns out that, on the basis of a set of assumptions

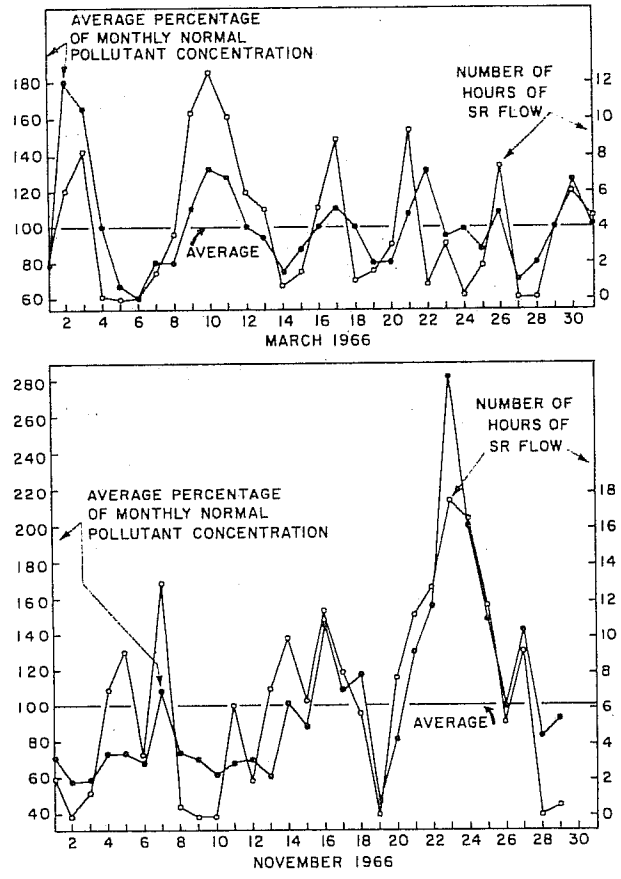

Figure 14. Hours of stable (SR) trace types during the day compared with the pollutant concentration during March and November 1966.

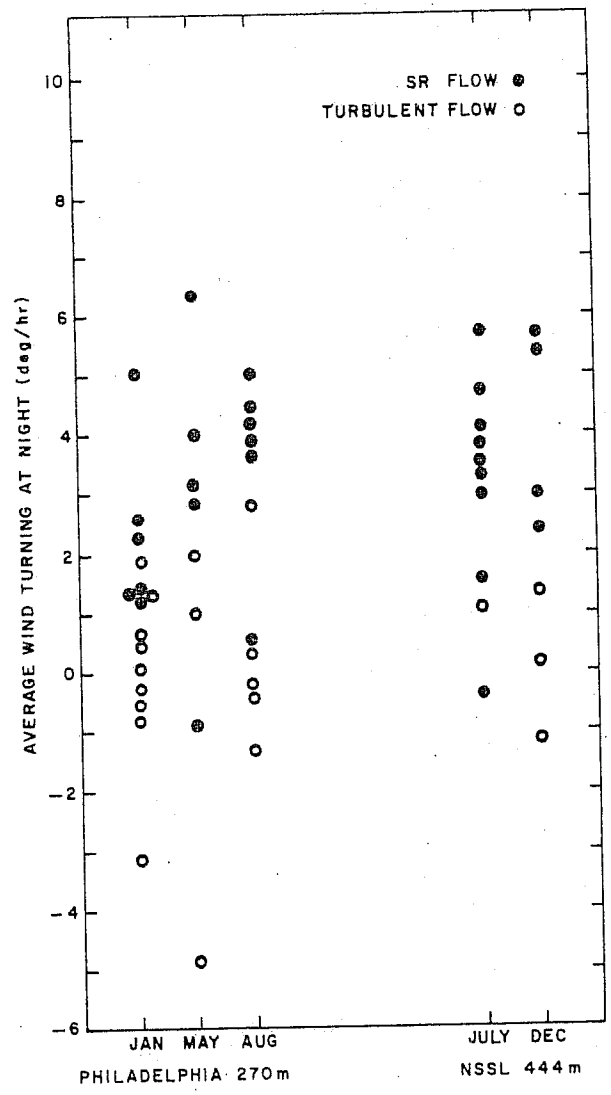

Figure 15. Relationship of stable (SR) and turbulent flow to the average wind turning at night.

B-79147

that seem, a priori, at least as plausible as those made by Prandtl, a flux-gradient relationship emerges so that in a region of unidirectional mean shear flow, such as the atmospheric surface layer, the flux components in the lateral and vertical directions are linear functions of the respective components of the gradient; this is not true of the flux in the down-stream direction, which is in fact given by a more complicated expression. This result does not depend upon stationarity of the flow or on linearity of the mean distribution of the transferred property, but it does, of course, depend on the assumptions introduced, which are, for the most part, not subject to direct experimental verification since they require measurements following individual fluid particles that are not technically feasible at this time. They can, however, be tested indirectly by rapid-response measurements at a single point, if certain assumptions can be made concerning the relationship between these "Eulerian" measurements and the "Lagrangian" measurements ideally required.

Two sets of data - one collected at Round Hill, Massachusetts, in 1961 and 1962 by Massachusetts Institute of Technology for the U. S. Army Electronics Command, and one collected at Liberal, Kansas, in 1967 by the University of Washington in conjunction with the Air Force Cambridge Research Laboratories - are being analyzed in an attempt to test these assumptions.

2.0 RESEARCH AT NATIONAL REACTOR TESTING STATION, IDAHO

2.1 Mesoscale Wind Field and Trajectory Studies

One of the prime concerns at the NRTS is the effect on the surrounding area of a planned or accidental release of radioactive material into the atmosphere. The obvious problem for the meteorologist is to determine where the material might be carried and how much it will be dispersed. If the data available for the task consist of long periods of wind records at a few stations, the logical approach is to establish a climatology of wind directions and speed. The problem of transport and dispersion may then be approached from the standpoint of modeled circulation based on climatology. Considerable work has been done with this approach (Dickson et al., 1967), and the relative dose factors obtained from the recirculation model are very enlightening. However, because it is very difficult to deduce the flow patterns of an area from one or two stations, a network of approximately 20 stations has been established to gather wind data in the boundary layer over the Snake River Plain including and adjacent to the NRTS, as shown in figure 16. The heights of the sensors vary from 50 to 200 ft above the ground. The overall objective is to use the data from this network to study the characteristics of the various mesoscale flow patterns in the boundary layer with the hope of gaining more understanding of the mechanisms involved in effluent transport and diffusion on this scale. The ultimate goal would be to establish a capability to forecast, with reasonable accuracy, mesoscale transport and dispersion. The immediate goal is to investigate methods of objectively analyzing the flow patterns by means of the network of wind stations. These analyses would expedite the computation of the advection of material in the flow and the application of numerical prediction techniques.

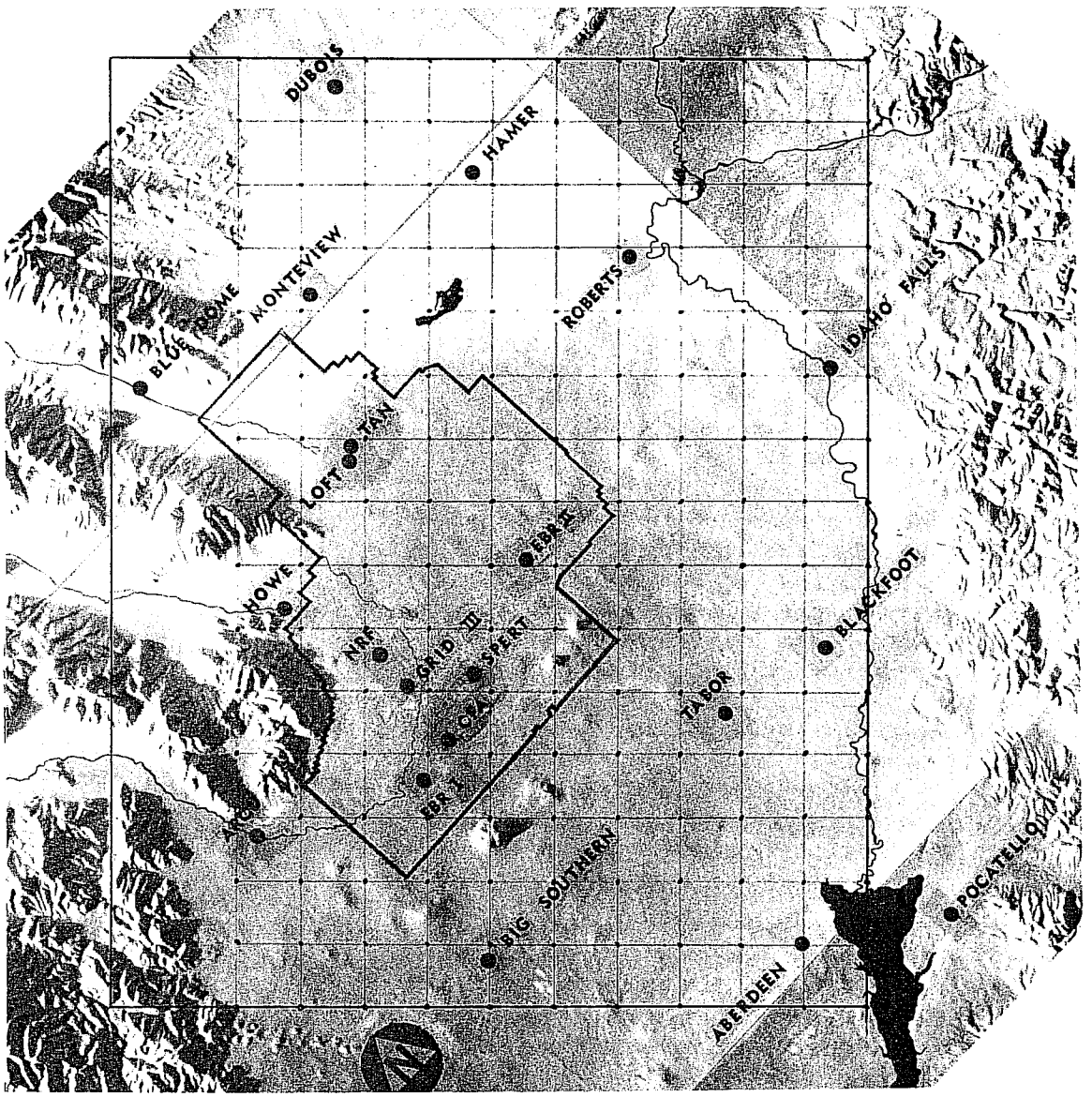

Figure 16. Mesoscale rectangular grid and network of wind stations on and around the National Reactor Testing Station, Idaho. The grid spacing is 6 mi.

B-79148 USCOMM - ERL

For convenience in numerical computation or prediction, it is advantageous to have data values defined on some sort of a regular grid system, usually rectangular. Since the positioning of the wind stations over the area of interest here is more or less random, the fundamental problem is to establish a scheme that will produce data values on regularly spaced grid points, based on the data values at the randomly spaced positions. One of the more refined schemes for accomplishing this task consists of fitting, by a least squares criterion, two dimensional functions of varying degrees of complexity to the data. For this, however, the network of randomly spaced stations must be fairly dense. The grid chosen for this preliminary study is shown in figure 16 superimposed over the network of wind stations within and adjacent to the NRTS boundaries. The spacing between the grid points is 6 mi. The grid has been oriented so that its columns lie approximately parallel to the change from smooth to rough terrain on both sides. This represents a rotation of + 49° from north.

Note in figure 16 that the wind stations are quite sparsely spaced especially in the upper left quadrant. It was the sparseness of the data that caused attempts at surface fitting to result in some very spurious wind fields. For this reason a much simpler approach was taken to the random-to-grid data conversion. The objective interpolation of the random wind data to the grid points established for testing in this study may be represented as

$$\bar{u}_{i,j} = \frac{\sum_{k=1}^{N} \frac{u_k}{r_k^n}}{\sum_{k=1}^{N} \frac{1}{r_k^n}} \quad \text{and} \quad \bar{v}_{i,j} = \frac{\sum_{k=1}^{N} \frac{v_k}{r_k^n}}{\sum_{k=1}^{N} \frac{1}{r_k^n}} \quad , \qquad (1)$$

where i and j are the coordinates on the grid, $\bar{u}_{i,j}$ and $\bar{v}_{i,j}$ represent the x and y components of the wind obtained at grid point, i, j, u_k, and v_k represent the x and y components of velocity at a wind station, r_k is the distance of the wind station from the grid point, n is an integer exponent that determines the strength of the weighting factor, and N is the number of wind stations that lie within a specified radius of the grid point at i and j. Note from figure 16 that for some points this scheme represents interpolation and for others extrapolation.

Some examples of this particular random-to-grid conversion scheme, with n 2 and a limiting radius of 36 mi, are given in figures 17 through 21. (These displays were entirely computer produced.) The data from the wind stations are shown in the form of standard wind symbols. Each full barb indicates a speed of 10 mph. The partial barbs are drawn to the nearest mile per hour. The winds at the grid points, resulting from the application of (1) to the data from the wind stations, are represented in vector form. The wind vectors start at the grid points and indicate direction of flow with their arrowheads and the speed of the flow with their lengths. A vector

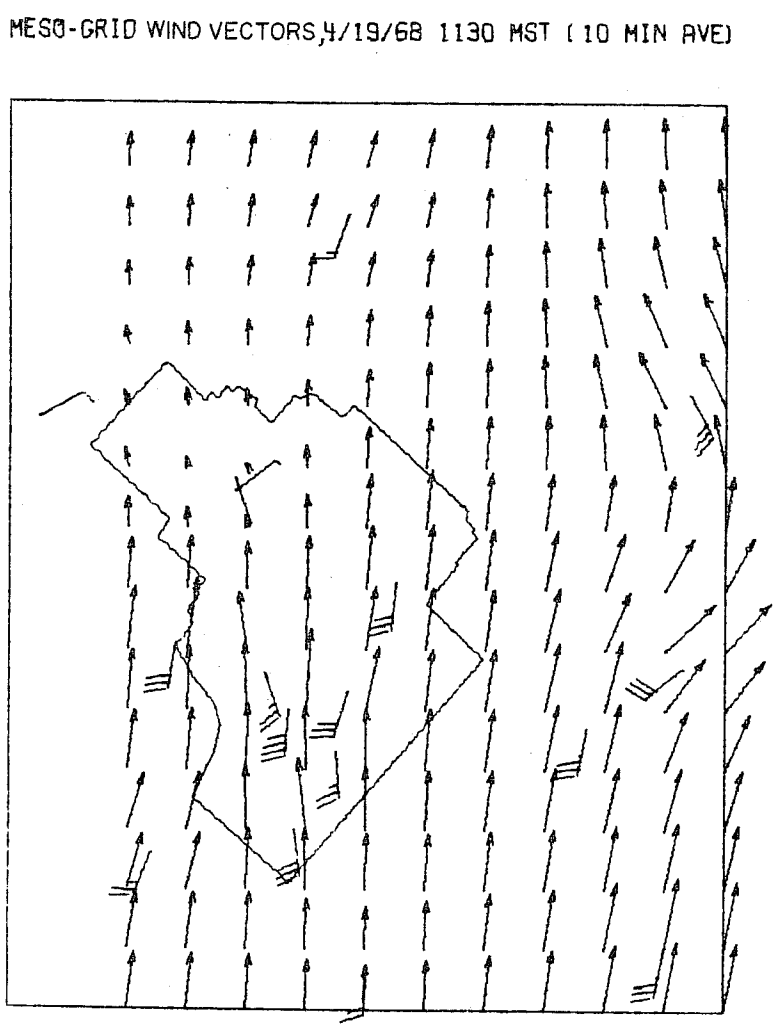

Figure 17. Mesoscale flow pattern depicted by wind vectors obtained from 10-min averaged winds indicated by the standard wind symbols. Averaging period ends at 1130 MST, April 19, 1968.

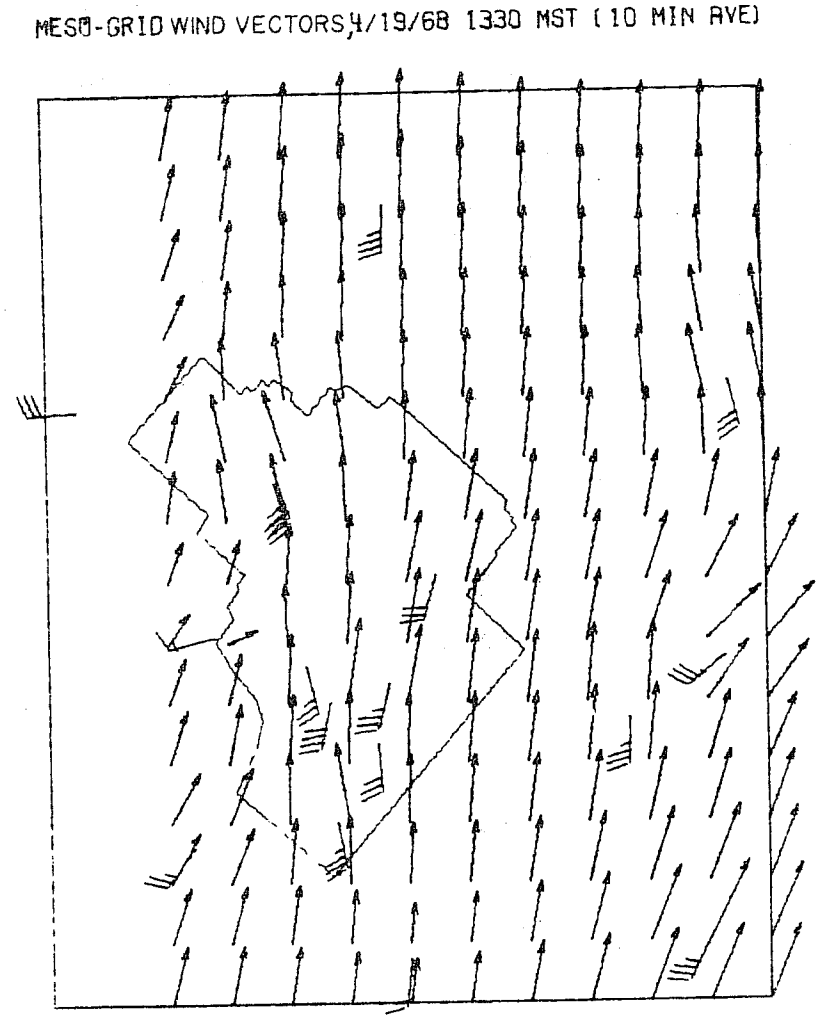

Figure 18. Mesoscale flow pattern depicted by wind vectors obtained from 10-min averaged winds indicated by the standard wind symbols. Averaging period ends 1930 MST, April 19, 1968.

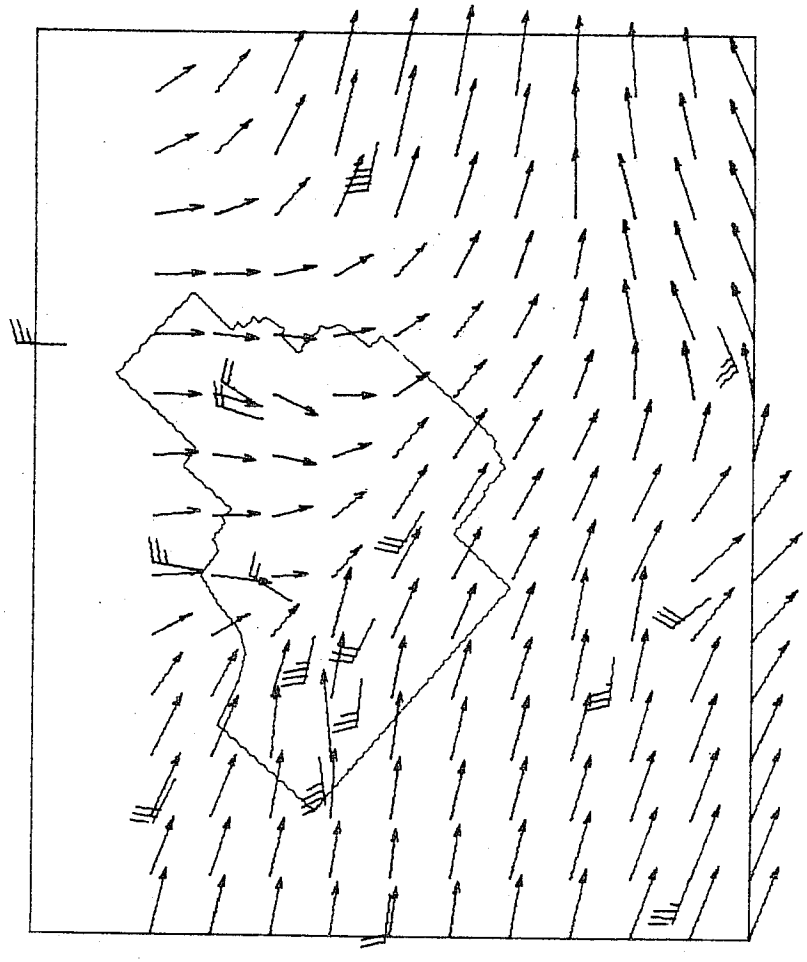

Figure 19. Mesoscale flow pattern depicted by wind vectors obtained from 10-min averaged winds indicated by the standard wind symbols. Averaging period ends at 1530 MST, April 19, 1968.

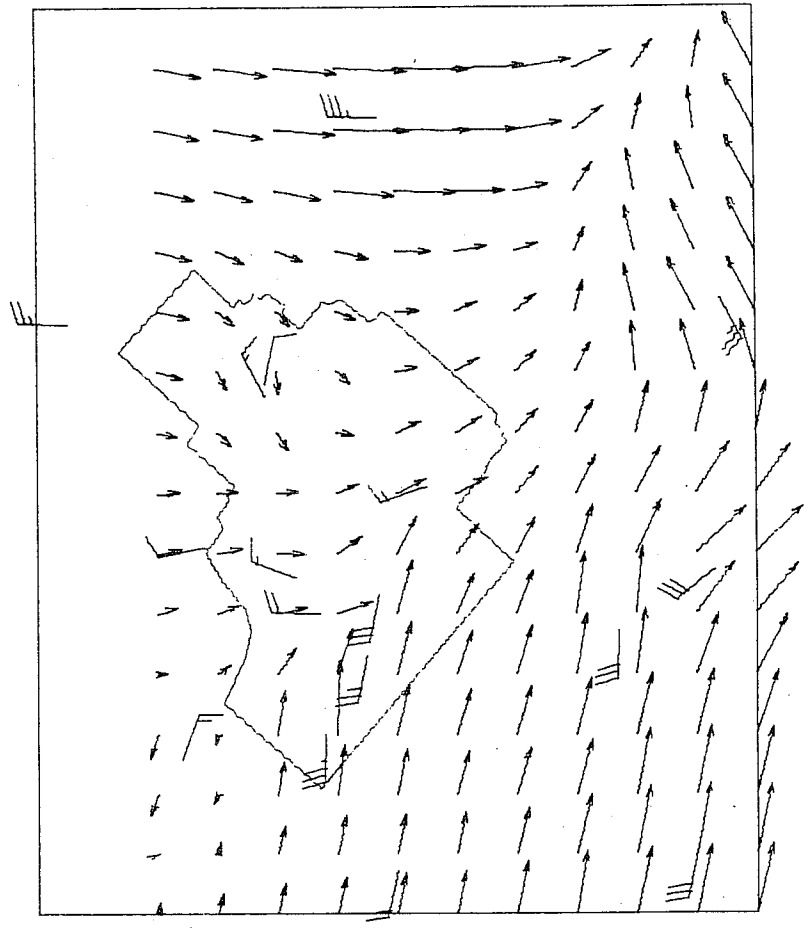

Figure 20. Mesoscale flow pattern depicted by wind vectors obtained from 1-hr averaged winds indicated by the standard wind symbols. Averaging period ends 1730 MST, April 19, 1968.

B- 79150

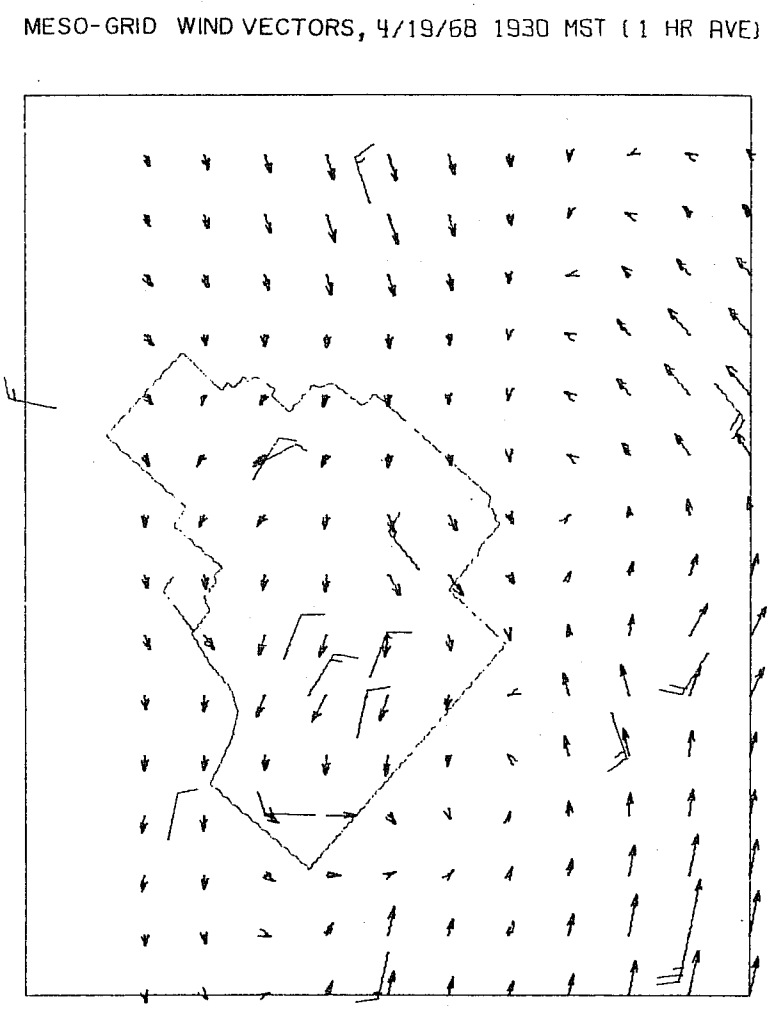

Figure 21. Mesoscale flow pattern depicted by wind vectors obtained from 1-hr averaged winds indicated by the standard wind symbols. Averaging period ends 1930 MST, April 19, 1968.

with a length equivalent to the distance between grid points indicates a speed of 25 mph. No data from the Monteview and Roberts wind stations were available during the time of this sequence, because the wind-sensing equipment had not yet been installed at these sites.

The series of flow patterns shown in figures 17 through 21 are spaced 2 hr apart. The first four wind fields are based on winds that were averaged over a 10-min period. In the last two wind fields, figures 20 and 21, the averaging time was 1 hr. During the period covered by this sequence a cold front moved through the area from the northwest. Its presence was first indicated on the 1330 MST display at Blue Dome, the station in the valley north of the site. The movement of the frontal system is accompanied by some interesting features in the gridded wind field. The shift of the wind at Hamer causes the instantaneous appearance of a zone of convergence 25 mi to the southeast. This indicates that the wind data from Monteview and Roberts are much needed. Another feature of the grid point winds obtained through (1) is the invariable reduction of the resultant velocities between station winds with opposing components, which would possibly result in unrealistically high values of convergence and therefore upward vertical velocities.

One method of checking the validity of the objectively obtained flow fields is to use them in constructing trajectories for comparison with actual trajectories of tetroons tracked through the field during the same time period. Such experiments are planned in conjunction with the radar testing and relative dispersion studies.

The technique for constructing trajectories is the standard one of interpolating the wind to the positions of the particles from the winds at the surrounding grid points and using an iterative scheme for advecting the particles. The trajectories shown in figures 22 and 23 are the result of simulated serial releases 1 hr apart with the same data represented in figures 17-21. The numbers at the ends of the trajectories indicate the order of release. These trajectories were constructed from winds averaged over 10-min periods and 10-min time steps for advection purposes. It was found, however, that hourly averaged winds and 10-min time steps for advection produced essentially the same trajectories. The effects of the changing wind field are portrayed well by these trajectories. Note that in the series released from EBR-I the strong southwesterly flow is reflected in the paths of the first two trajectories, with trajectories from the next two releases shifting slightly northward. The effects of the frontal passage are indicated first in the latter portion of trajectory 4 and then by the southward veering of 5 and 6. In the set of trajectories released from the LOFT site, shown in figure 22, the strong southwesterly current carries the first five trajectories out of the range of interest before the frontal passage indicated by the path of trajectory 6.

One obvious application of the mesoscale flow patterns and trajectories would be in obtaining relative dose factors with the same techniques as before (Dickson et al., 1967), but replacing the model winds with the objectively analyzed winds from the grid. This could be done with past wind

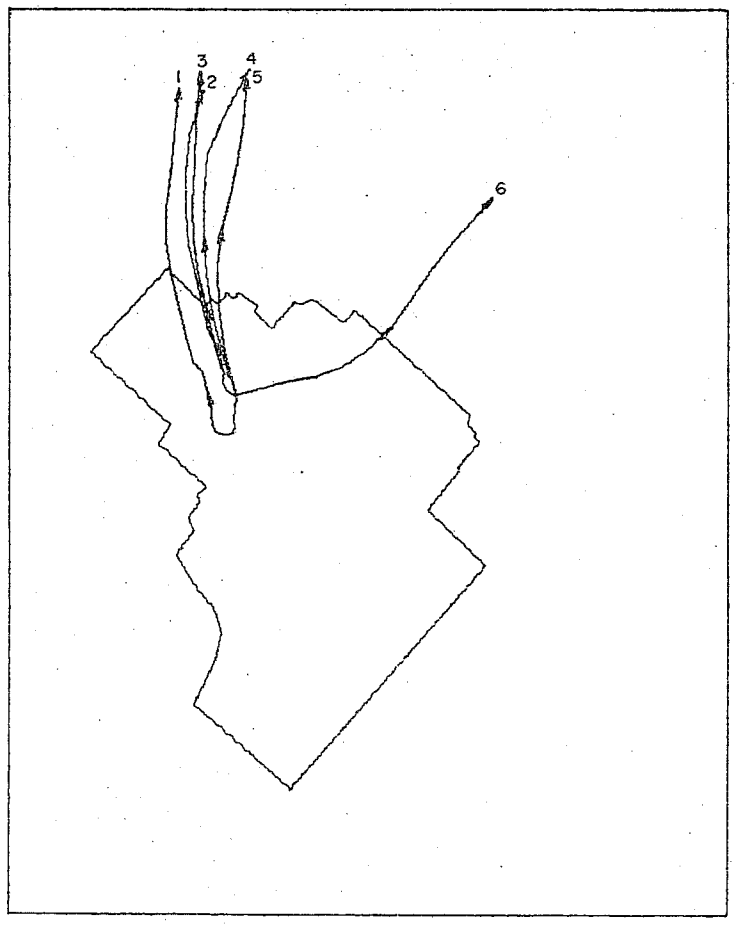

Figure 22. Trajectories constructed from the objectively obtained flow patterns by serially releasing hypothetical particles at 1-hr intervals from the LOFT area.

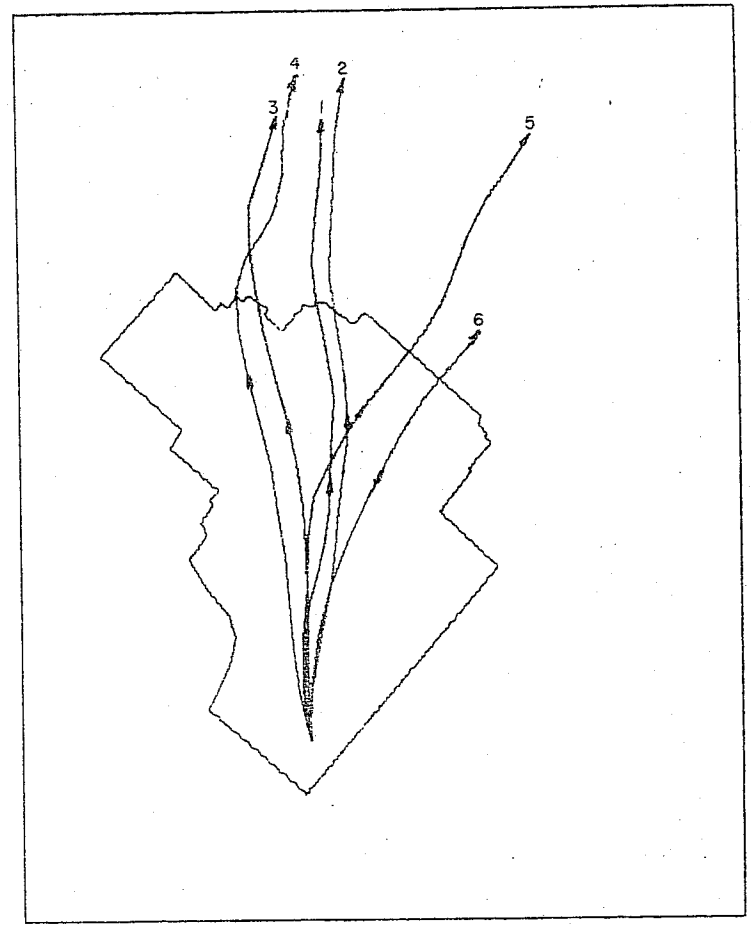

Figure 23. Trajectories constructed from the objectively obtained flow patterns by serially releasing hypothetical particles at 1-hr intervals from the EBR I area.

B- 79152

records to establish a climatology. With telemetered data and a reliable forecasting scheme, the technique could serve in emergency situations to provide early warning of impending contamination.

The dynamic effect of warmer air riding up over the leading edge of a cold front has not yet been considered. The complexity of the problem will require special consideration and experimentation. The primary objective at present is to determine the validity of the objectively determined wind fields. It is obvious from this initial example that data from the Roberts and Monteview stations are essential. Data are now available from Dubois and a new station approximately 6 mi south of the TAN area. It should be mentioned here that bad data usually are more apparent when viewed in the perspective of time series of the automated displays. A number of errors in the data have been found because of obvious inconsistencies in the flow patterns.

As mentioned, experiments are planned in which constant density tetroon flights will be tracked and compared with trajectories constructed from the wind fields. Wind and temperature soundings are also planned during these experiments to gain information about the connection between the synoptic and mesoscale flow. This data along with analyses of such properties of the flow field as divergence and vorticity will suggest the means by which the most realistic representation of the flow may be obtained.

2.2 Radar

The reliability of turbulence and diffusion statistics determined from free floating targets, tracked by radar, can be seriously affected by the tracking accuracy of the radar. Analytical expressions for estimating the gross effect of this type of error on such quantities as velocity variance have been derived (Ohnsorg, 1957, de Jong, 1958). One of the basic assumptions was that the error was ramdom in nature. Experimental data from simultaneous tracks of single balloons with two radars provided estimates of tracking error for WF-2 radars (Laby and Sparrow, 1965). The balloons were skin-tracked with the aid of an attached reflector target. Resultant error in height speed and angle of wind vector were calculated from the expressions derived by de Jong.

The effect of varying degrees of random tracking error on the turbulent characteristics of a free-floating target were studied by superimposing a random error onto the range azimuth and elevation readings from a smoothed trajectory (see last semiannual report). For the M-33 the rms values specified for the error in range azimuth and elevation readings were 5 yards, 0.075^{o} and 0.075^{o}, respectively. The effects of the superimposed random error and attempts to eliminate it by a smoothing process were readily apparent when the autocorrelation functions for the velocity components were compared. The addition of a random error bounded by $\pm 2\sigma$ to the tracking data altered the autocorrelation functions beyond the point of recognition. A 3-min smoothing of the data did not significantly alter the turbulence

(primarily because the data were already smoothed over this interval), and it did not eliminate enough of the effect of the error. A 7-min average eliminated most of the effect of the error, as evidenced by the close coincidence of the autocorrelation functions, but the turbulent motion seemed to be altered significantly.

The results of this preliminary investigation, although instructive, are based on two limiting assumptions: a) that the rms values specified for the errors are still valid after normal deterioration of the electronics components of the radar as well as being valid for transponder tracking and b) that the tracking error will be of a random nature. Because of this and the fact that the M-33 fire control radar, along with the tetroon-transponder system, has been used and may yet be used to study relative turbulence and diffusion in the atmosphere, an attempt is made here to study the nature of the tracking accuracy of this system.

The two radars used in this experiment were carefully positioned by a ground survey. They were separated by a horizontal distance of 25,298 yd (14.37 mi) and by a vertical distance of 1484 ft because one of the radars was placed on a butte for possible emergency purposes. One objective was to test the radars for systematic errors by checking the errors and discrepancies in the radar locating of stationary transponders at known positions. The next objective was to test the tracking capabilities by examining the discrepancies obtained in following a single tetroon-transponder system simultaneously with both radars.

One of the first sources of error that became apparent during the stationary tests was the manual reading of the dials to obtain the range azimuth and elevation angles. The spacing between graduated markings on the dials is 5 mil for elevation and azimuth and 5 yd on the range dial. This means that the readings are subjectively estimated to the nearest mil and nearest yard. One mil is 67 percent of the rms error specifications for azimuth and elevation and 1 yd is 20 percent of the rms error specification for range. The magnitude of the target velocity error for an interval of 30 seconds between readings is about 1 m/s.

For the portion of the test involving the stationary target, six surveyed locations were selected for transponder placement. However, only four locations were observable from both radars. In what follows, the radar located at the Central Facilities Area of the NRTS will be referred to radar No. 1 and the radar located on the East Butte will be designated radar No. 2. The results of the stationary positioning are summarized in table 2.

Table 2. Positioning Errors for Stationary Targets

	Radar No. 1			Radar No. 2		
Station	E_R(yd)	E_θ(mil)	E_φ(mil)	E_R(yd)	E_θ(mil)	E_φ(mil)
1	117	-0.13	1.85	156	-0.40	-0.93
2	152	-0.17	-0.76	165	-7.30	-3.68
3	124	-1.88	-1.85	150	1.49	+0.36
4	219	0.97	2.46	175	-2.59	-1.53
5				165	-2.77	-1.43
6				142	-1.52	-2.57
Mean	153	-0.30	+0.42	159	-2.18	-1.63
Std. Dev.	40.1	1.02	1.71	10.8	2.71	1.24

The average range error, E_R, for both radars is about +150 yards. Plotting E_R against range for both radars indicates that the major portion of the error is independent of the range. This would indicate that most of the error is due to the time delay required to trigger the transmitter in the transponder, which is independent of the distance of the transponder from the radar. Refraction of the signal will also cause a positive range error, but its magnitude would be dependent on the range. If we compare the standard deviation of the range errors with the rms specification we find a factor of four excess for radar No. 1 and a factor of two excess for radar No. 2. Noting that the rms error specification for azimuth and elevation angle readings is 1.34 mils, we find the only significant departure from this in the azimuth reading from radar No. 2. The departure seems to be attributable to the reading taken on station No. 2. There is the possibility that the error in this value includes a 5 mil error due to the manual reading. Three of the ten sightings, station No. 1 by both radars, and station No. 2 by radar No. 1, were carried out three times each to verify the dial readings. It may be noted that the azimuth errors are minimal for these cases. The large mean errors in the azimuth and elevation readings for radar No. 2 are attributable to the radar not being leveled just prior to the test.

Table 3. Positioning Error for Stationary Targets

Station	Range From Radars (yd)		Horizontal Error (yd)		Horizontal Discrepancy (Yd)
			Radar 1	Radar 2	
1	1	5,604	32.4	18.6	57.0
	2	30,149			
2	1	7,773	2.3	198.5	199.5
	2	27,625			
3	1	34,620	69.0	55.5	123.2
	2	40,549			
4	1	45,774	81.0	104.8	176.7
	2	40,159			
Mean			46.2	94.3	136.6

The effect of these errors on the horizontal radar positioning of the targets is shown in table 3. The radar located positions were computed with range readings corrected by 150 yd for both radars. Note that, with the exception of the radar positioning error at station 2, all the errors in horizontal positioning are much less than 1 percent, and in this connection we should recall that the reading of the azimuth angle for radar No. 2 at station 2 was subject to question. The errors in the vertical positioning were of similar magnitude. Thus as an instrument for determining the position of a stationary object we might expect an accuracy of at least 0.25 percent, which is more than adequate for many purposes.

However, if one wishes to determine the velocity of a moving object, positioning errors of the order of those in table 3 occurring randomly from reading could cause very large errors, depending on the time interval between the positionings. For studying the smaller scale characteristics of Lagrangian turbulence and diffusion, time intervals of 30 s to 1 min have been used (Angell, 1962; Angell, Pack, and Dickson, 1968; Kao and Wendell, 1968). This would mean that the positioning errors discussed would cause velocity errors of up to 7 m/s. To reduce this error running averages of up to 3 min have been applied. This process would significantly reduce the effect of errors with magnitudes of those shown in table 3.

To study the magnitude and characteristics of the positioning errors that arise in following a moving target, one encounters the difficulty of not knowing the exact positions along the trajectory. However, if the moving target is followed by two radars simultaneously, one may study the magnitude and characteristics of the discrepancies in position and the derived velocities. This type of experiment was carried out for a single tetroon flight on the same day as the positioning experiments with the stationary targets. The general characteristics of the discrepancies are shown in table 4. The means and standard deviations are based on 392 observations by each radar separated by 30-s time intervals.

Table 4. Comparative Data for Two-Radar Single-Tetroon Test

	Radar No. 1	Radar No. 2
Beginning Range (yd)	8,400	27,145
Ending Range (yd)	65,136	50,550
Mean Range Difference (yd)	-13.2	
Mean Azimuth Difference (deg)	0.0160	
Mean Elevation Angle Difference (deg)	- 0.102	
σ_R	51.1	
σ_θ	0.132	
σ_φ	0.129	

We may note here again that the large discrepancy in the mean difference in elevation angle may be attributed to the leveling accuracy of one of the radars. We may also note that the rms values for the azimuth and elevation angles, σ_θ and σ_φ respectively, are quite close to each other but about a factor or two larger than the common value specified for the error. The rms value for the range, however, is larger by a factor of 10 than the error value specified.

If we assume that the tracking characteristics for both radars is the same, then the rms values for the error in both radars is the same. If we also assume that the errors are random and therefore uncorrelated, then the rms values for the radar error may be obtained from the rms values of the discrepancies between the radars as follows:

$$\sigma_e = \frac{1}{\sqrt{2}} \sigma_d \cdot \qquad (2)$$

Applying this result to the values in table 4, we obtain the estimate for the rms error values, σ_R = 36 yd, σ_θ = 0.093°, σ_φ = 0.091°. These results indicate that by far the largest deviation from the specified rms error values occurs in the range readings. This deviation is about a factor of 7, while the errors in the angular readings were about 20 percent in excess of the specified rms values. It should be kept in mind that the rms values for range error were specified for skin tracking and that the values presented here are for transponder tracking.

To study the seriousness of the effects of the errors on turbulence and dispersion information, which may be obtained from the data, time series of position and velocity discrepancies were computed. They are presented in figures 24 through 29 and summarized in table 5. The orientation of the coordinate system for these results is such that the y coordinate is positive toward the north and the x coordinate is positive toward the east. Note from the values in table 5 that the running average reduces the standard deviations by varying amounts.

Table 5. Position and Velocity Discrepancies for Dual Tracked Tetroon Transponders

	Mean	Standard Deviation	
		No Smoothing	5 point (2 min) Smoothing
Δx (m)	49.9	78.3	69.9
Δy (m)	33.9	58.1	50.9
R_h (m)	104.5	47.4	41.3
Δz (m)	- 54.7	83.6	67.1
u_1 (m/s)	4.1	2.1	2.0
(u_2-u_1) (m/s)	0.0	1.6	0.4
v_1 (m/s)	2.4	1.5	1.3
(v_2-v_1) (m/s)	0.0	1.3	0.3
w (m/s)	0.1	1.0	0.5
w_2-w_1 (m/s)	0.0	2.2	0.6

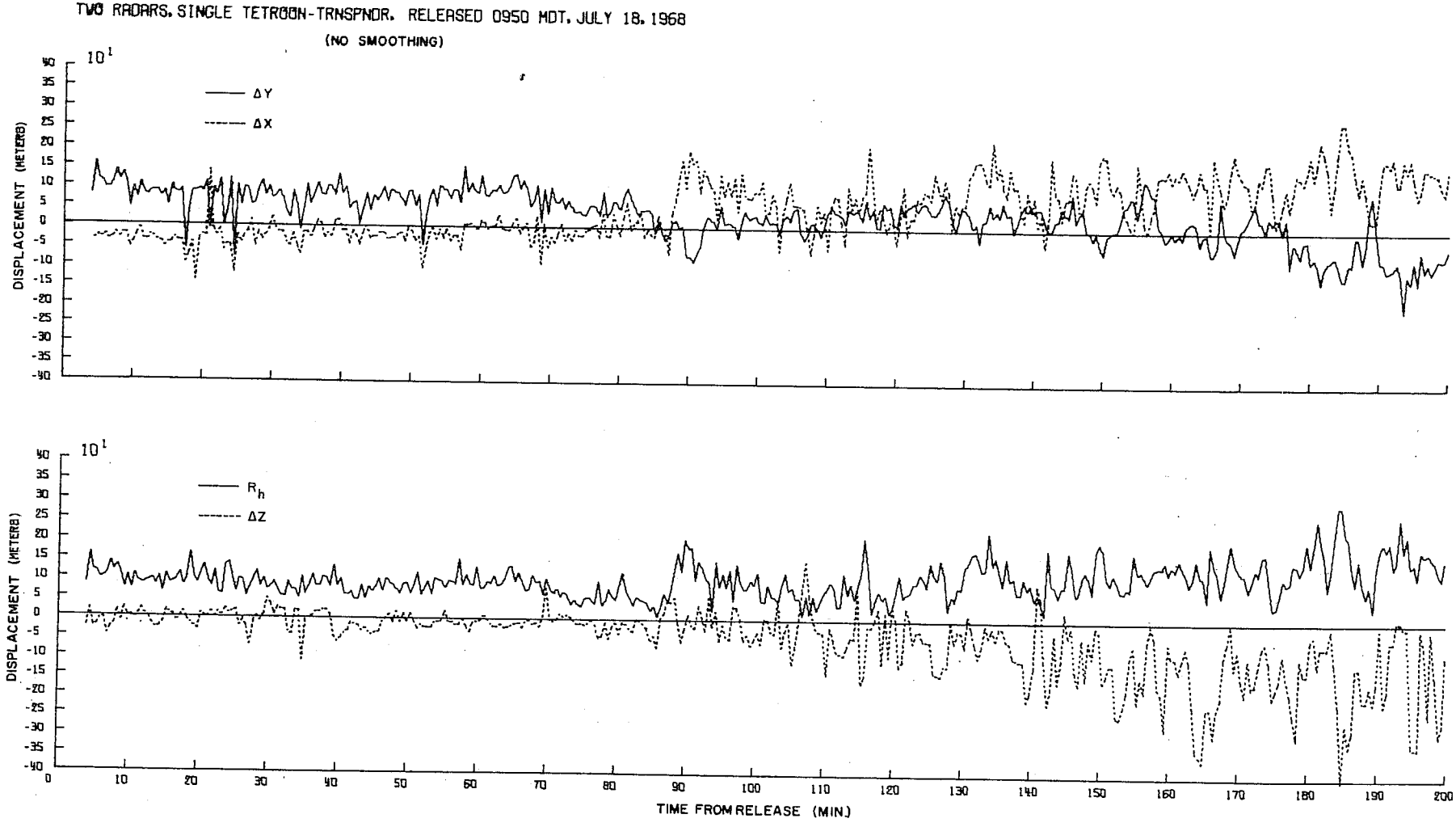

Figure 24. Time series of discrepancies in the coordinate positions of a single target as determined by two separate M-33 radars. The horizontal displacement R_h is computed from Δx and Δy. These plots are for the original data, with no smoothing applied.

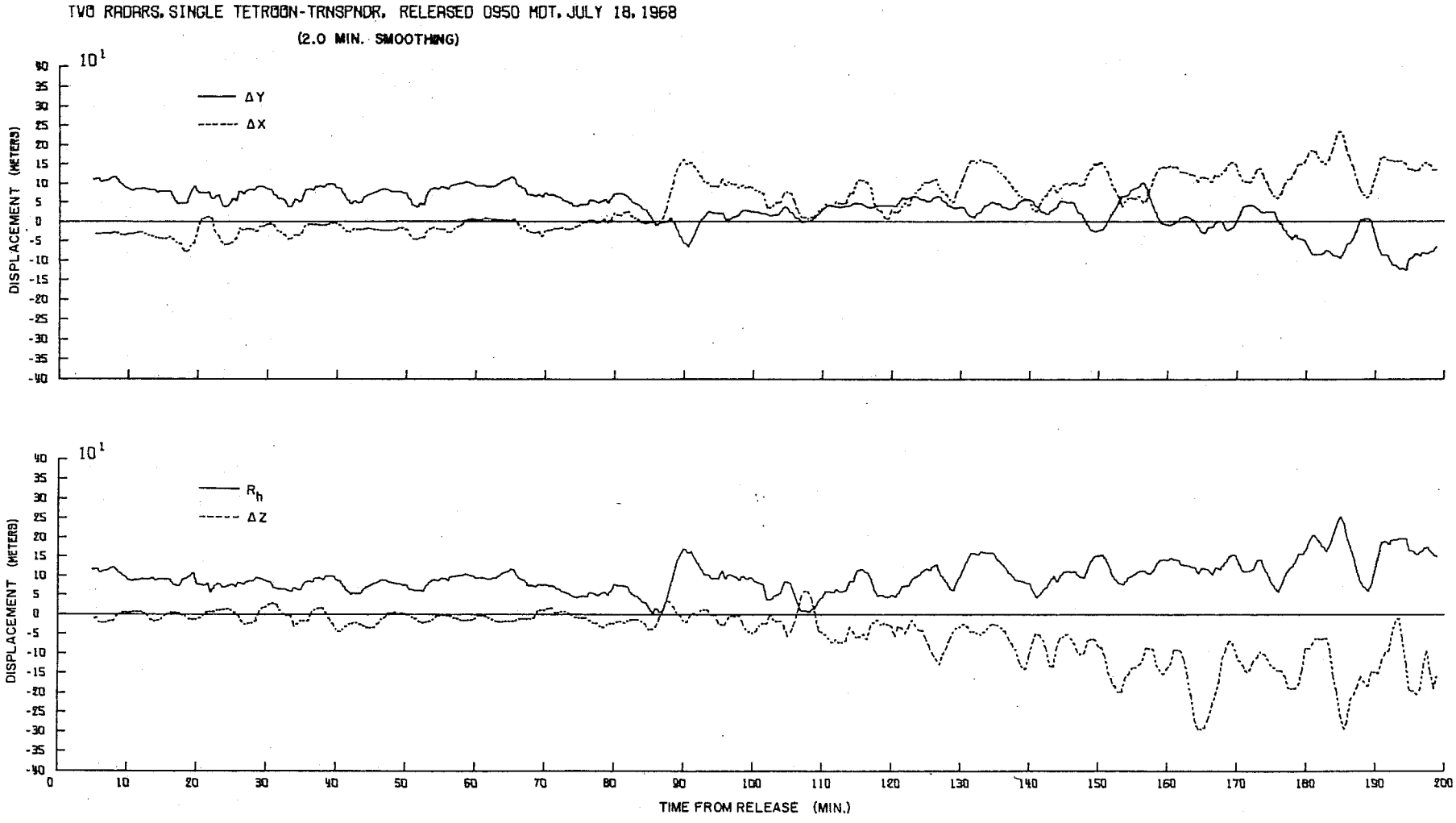

Figure 25. Time series of discrepancies in the coordinate positions of a single target as determined by two separate M-33 radars. The horizontal displacement R_h is computed from Δx and Δy. These plots are for a 2-min (5 point) running average applied to the original data.

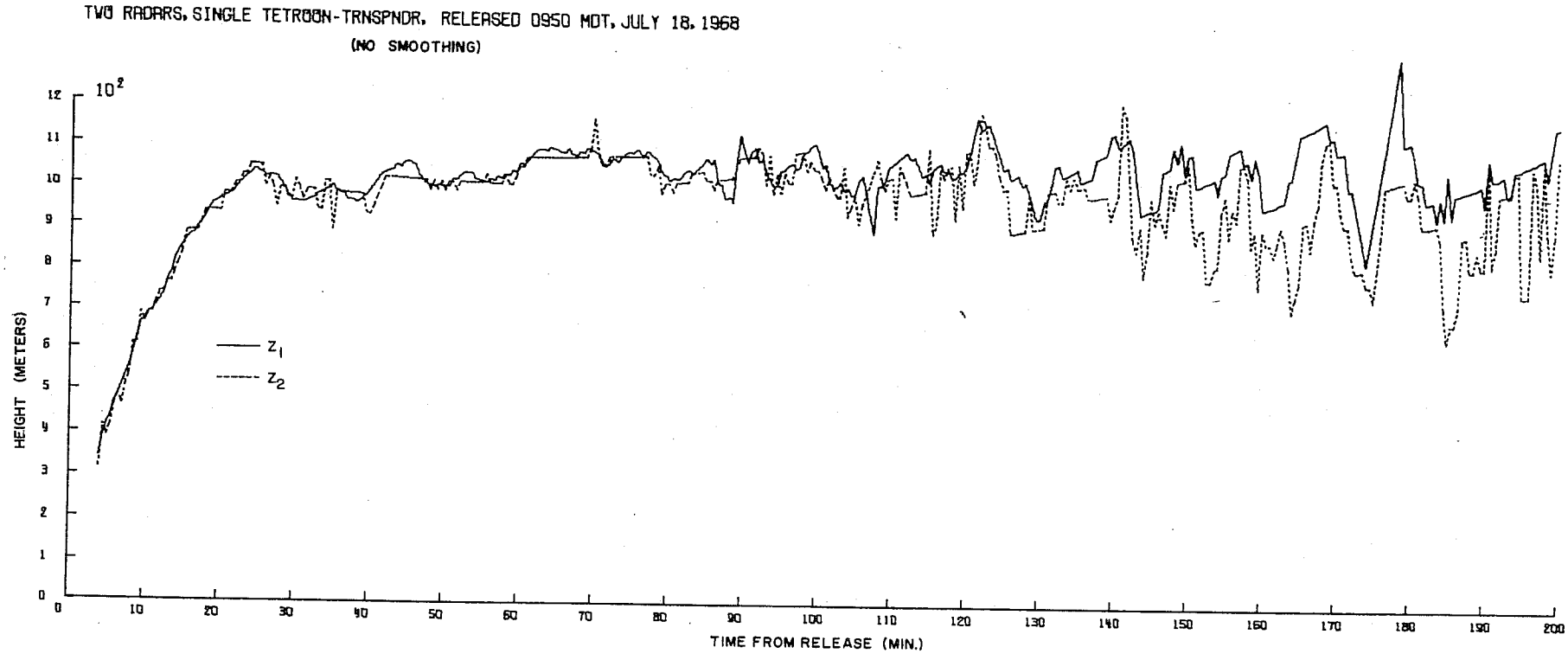

Figure 26. Time series of height values of a tetroon determined simultaneously by two M-33 radars. No smoothing has been applied to the original data.

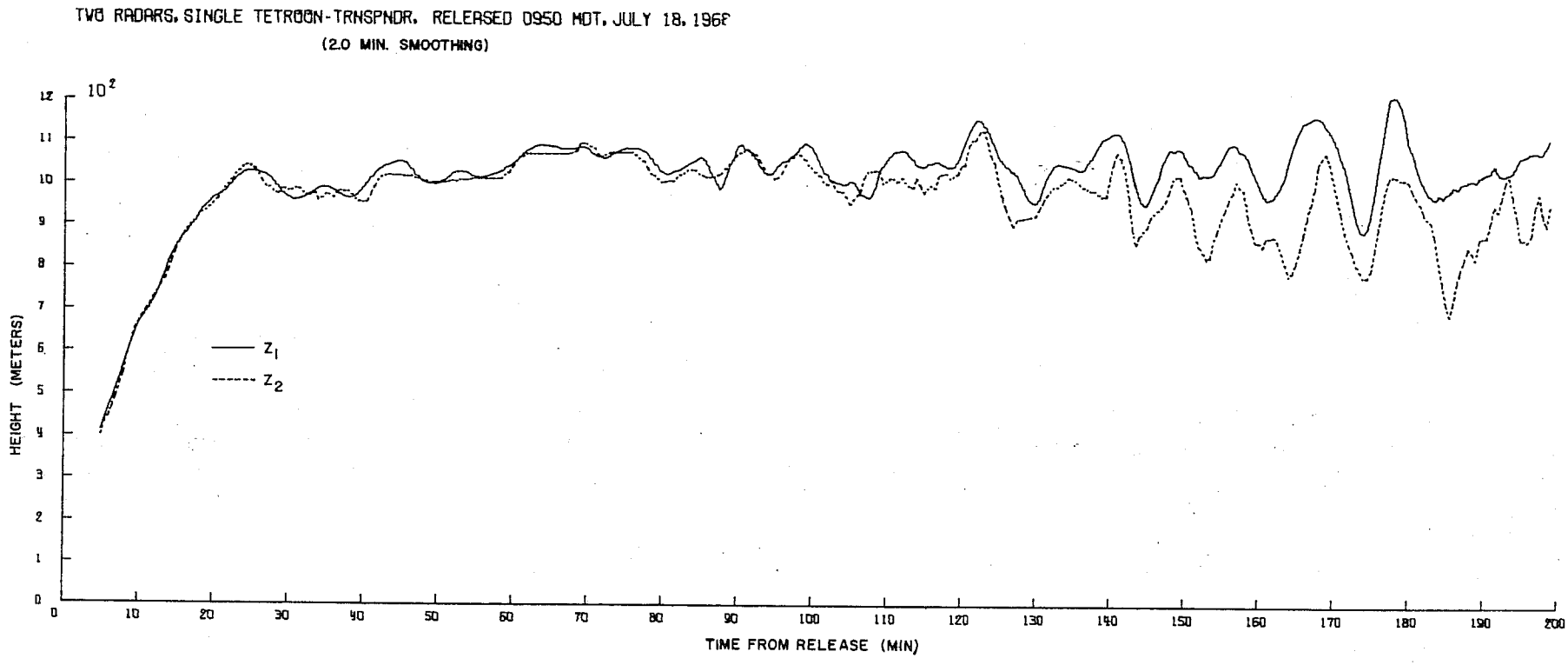

Figure 27. Time series of height values of a tetroon determined simultaneously by two M-33 radars, with 2- min smoothing of the original data.

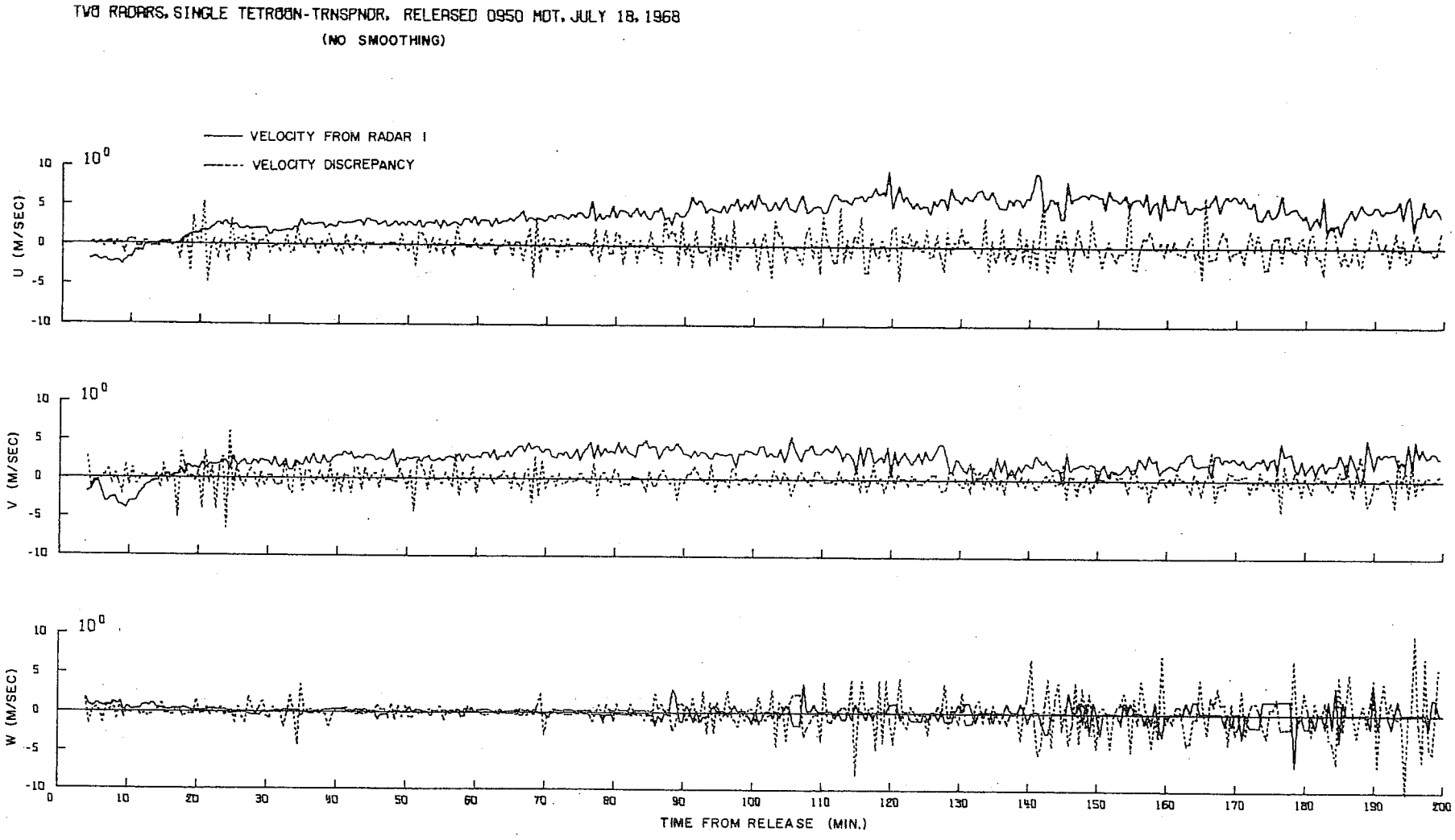

Figure 28. Time series of component velocities of a tetroon as determined by radar 1 and the discrepancies between these velocities and those determined by radar 2. No smoothing has been applied to the original data.

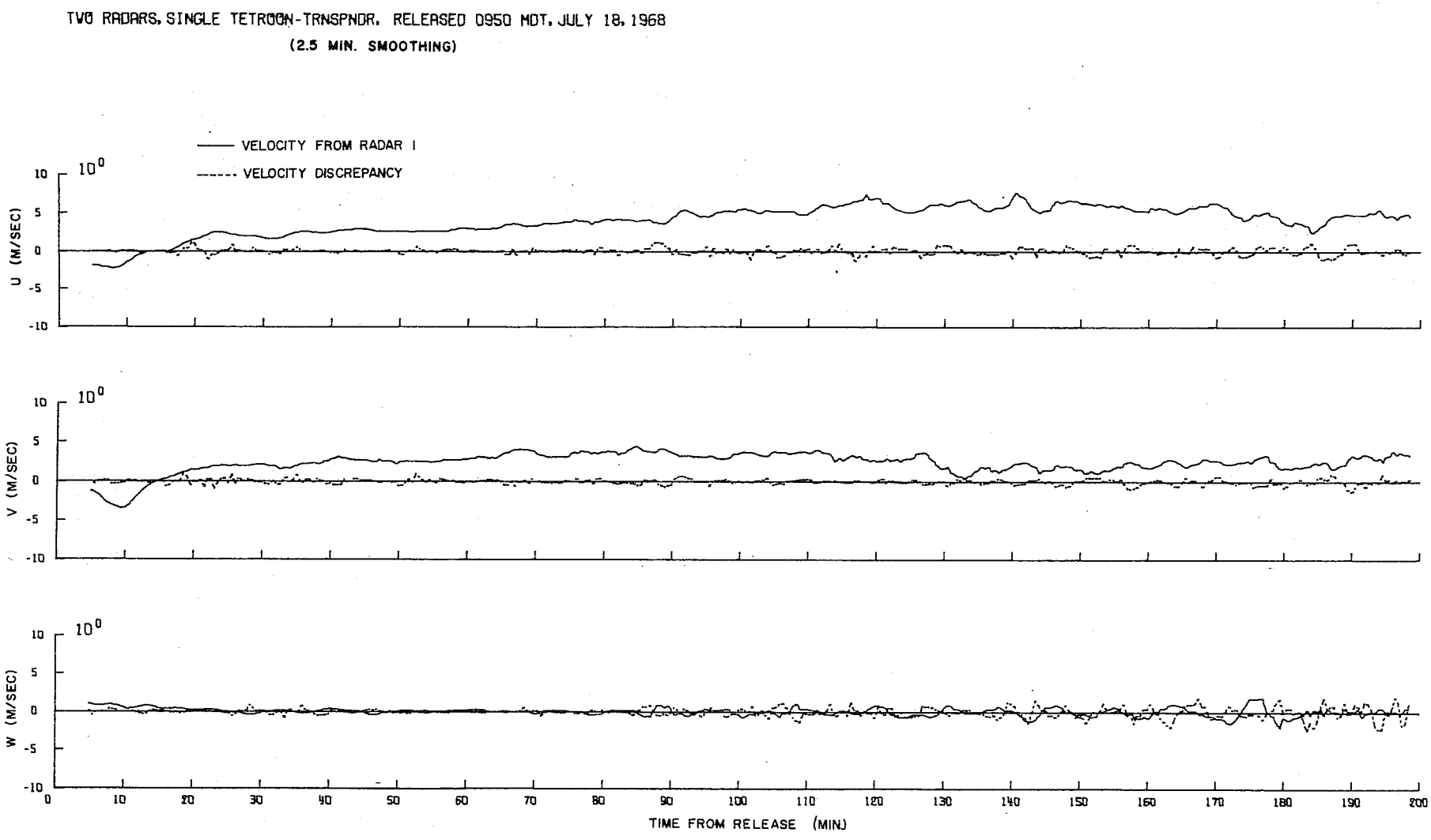

Figure 29. Time series of component velocities of a tetroon as determined by radar 1 and of the discrepancies between these velocities and those determined by radar 2 with a 2.5 min (5 point) smoothing of the original data.

The standard deviation of the discrepancies in particle position is reduced only 10 to 20 percent. From figures 24 and 25 we see that the primary reason for this are the trends throughout the period the data were taken. The horizontal components of velocities for radar No. 1 also show small reductions in standard deviation due to the 5 point averaging, but the discrepancies between velocities determined from both radars show reductions in standard deviation of about 75 percent. The discrepancies in the vertical velocities are reduced by about 70 percent, but the standard deviation of the vertical component of velocity determined by radar No. 1 is reduced by 50 percent.

To get a better picture of the discrepancies of position and velocity in relation to the motion itself, and the effect of smoothing on both, we may examine the time series of these quantities in figures 24 through 29. From figure 24, showing the position discrepancies in the horizontal and vertical direction as well as the discrepancy in the resultant horizontal, we see that the fluctuations in the discrepancies consist in part of some rather random fluctuations near the folding frequency (1 cycle/min). The cause of these rapid fluctuations seems to lie in the searching characteristics in automatic track mode of the radars. The radar allows the target approximately $\pm$ 2 mils of latitude from the center position in both horizontal and vertical direction before correcting the antenna direction to strengthen the signal being received. This characteristic is easily observed when the target is in range of the optical system of the radar.

The phenomenon is reflected in the first 80 min of vertical position data shown in figure 26. The solid curve is the unsmoothed plot of height against time, as determined by radar No. 1. The dashed curve is the same plot for radar No. 2. During this portion of the flight, azimuth and elevation positioning of the target from radar No. 1 was done with the aid of the optical system because of the close proximity of the target. Since the target was never within the range of the optical system of radar No. 2, the positioning was done in automatic mode. Note that the vertical change in position as sensed by radar No. 1 is much smoother than that sensed by radar No. 2. However, in figure 27 we observe that a 2-min (5 point) smoothing, while causing almost no perceptible difference in the solid curve, brings the agreement between the two curves considerably closer.

The searching motion of the antenna of radar No. 2 caused a certain amount of subjectivity in reading the dials at specific instants in time. During the first 80 min of the flight the antenna motions of radar No. 2 seemed to begin every 1 to 3 s. Thus, for a large percentage of the readings, the dials were in motion at the end of each 30-s interval. The dial readings of elevation angle from both radars in automatic track mode indicated periods of 2 to 5 min in which the elevation angles seemed to be biased toward persistence. These periods show up in the height traces as straight-line segments with relatively small positive slopes. The slopes of the lines depend on the rate of range change during the period. They are flat for radar No. 2 during the early portion of the flight because the target was moving tangentially with respect to the radar's position.

During the last hour of the tracking, the positioning by both radars was done electronically by the balancing of the height of two spikes on signals displayed on cathode ray tubes. This introduced further subjectivity into the readings and appeared to cause drastic errors in the results, as evidenced in the dashed curve in figure 26.

The five point (2-min) smoothing seems to be effective in removing the rapid oscillations in the position discrepancies (figs. 24 and 25), but some interesting features in the positioning discrepancies remain. The trends in the x- and the y- as well as the z-position discrepancies are attributable to radar No. 2 not being level, but the oscillations of approximately 10-min periods during the last half of the flight are more difficult to explain. The oscillations in the smoothed vertical height discrepancies seem to be associated with a combination of slight changes in phase and frequency of the oscillations, with approximately 10-min periods, in both the smoothed traces of vertical height shown in figure 27.

The residual oscillations in horizontal discrepancy are of such amplitude that they cause velocity discrepancies of usually less than 1 m/s. As figure 28 shows, the serious velocity discrepancies are due to the rapid fluctuations that are effectively reduced by the smoothing. The effect of the smoothing on the velocity discrepancies is evident from figures 28 and 29, which show that tracking accuracy is most critical for the vertical velocity, especially in stable situations, because it is smaller than horizontal velocity.

One of the questions under investigation is how significant the tracking error is in determining relative turbulent motion and the consequent diffusion. If we compare the variances of the velocity discrepancies with the average variances of the relative velocities from 10 pairs (Kao and Wendell, 1968) we find them to be about an order of magnitude smaller. Admittedly, more dual tracking data are needed to make such a comparison valid but at least one is encouraged to go further in determining the capability of the radar-tetroon-transponder system to measure the relative turbulence and dispersion characteristics in the boundary layer.

For convenience, we may summarize the findings at the present stage as follows:

1. The time delay required to trigger the transmitter in the transponder causes a positive error, which is independent of the distance from the radar, in the range indication from each transponder. A correction may be determined for each transponder and applied to the tracking data.

2. The signal from the transponder causes a fluctuation, with an amplitude of about 30 yd and a period of about 2 s, in the range reading from a stationary target.

3. Tracking data obtained periodically from manual readings of the range azimuth error are subject to errors because of a) coarse resolution of the dial markings, b) misinterpretation of a dial mark, c) bias toward persistence for readings during periods of oscillatory

variation, and d) nonsynchronous readings of the three separate dials. Digitization and automated recording of the tracking data should eliminate these problems.

4. In tracking a transponder, the most serious error, in comparison with the specified rms error values, occurred in the range indication. The estimated rms error value for the range was seven times the specified value, but the values for azimuth and elevation angles were only 20 percent larger than those specified.

5. A running average of the position data is quite effective in reducing the velocity discrepancies caused by high frequency random type fluctuations in position discrepancies. The residual velocity discrepancies are small compared with the tetroon velocities, and indications are that they may be small compared with relative velocities of the scale to which tetroons are sensitive. This may be determined in the next series of experiments with the digitized readout of the data.

The primary accomplishment so far has been establishment of the logistics and computatonal schemes with which the accuracy of a tracking system may be examined in detail. The radars are now being modified and equipped to digitally record the tracking data on paper or magnetic tape. This should eliminate the subjectivity and inefficiency of reading the dials and will also allow much more rapid sampling of the data, which should reduce the errors due to searching characteristics of the radar. When the radars have been modified, more experiments are planned with dual tracking of a single target, as well as with pairs and clusters.

2.3 Evaluation of Solid-State Transponders

Forty-five solid-state X-band 403-MHz transponders, manufactured by the Cordin Company of Salt Lake City, were tested and evaluated. Static in-shop and distance checks were performed on these transponders. The static distance checks were made across a 26-mi baseline extending from the radar to the north end of the NRTS. The static distance check consisted of serial triggering of the transponders with the M-33 pulse and checking whether the M-33 automatic tracking system would "lock" onto the emitted transponder signals. Of the 45 units tested, only five failed to meet the static distance testing. The serial numbers of these five units were TT6-97, 192, 175, 80, and 153. These same five units (discussed further below) did not respond to the static bench check originally.

For each successful transponder static distance check the corresponding M-33 operational characteristics and transponder variables were recorded. These data are summarized in table 6.

The in-shop static tests were performed with the following standard test equipment: A Tektronix Model 533A oscilloscope with L-20 plug-in unit (spectrum analyzer), model D-151776 portable X-band transmitter, shop-made pulse modulator, MX-24/APR-1 radio receiver with TN-3B/APR-1 tuner, Cordin Company radio receiver (S# 147), Delta Design, Inc. temperature test chamber (S# 1222),

a Simpson model 169 VOM, a Simpson model 379 battery tester, a Dumont oscillograph-record camera, type 297 (S# 5A98), and an especially arranged test chamber in which each transponder was energized and tested separately. This chamber measures 48" wide x 38" high x 28" deep, is lined with aluminum and copper foil, and covered with 1-inch thickness of horsehair impregnated with polyester resin and lamp black. The lining is to alleviate any images or reflections that might affect the various transponder test measurements.

Table 6. Summarized Static Distance Evaluations of M-33 and Transponder Performance

	Range	Magnetron Current	Relative Signal Strength	Band Width
Average	45,717 yd*	2.1 mA	- 16.6 dB	1.4 MHz
St. Deviation	± 20 yd	± .834 mA	± 2.5 dB	± .238 MHz

* May be a question on atmospheric conditions.

As mentioned, five of the original 45 units would not respond. Minor tuning of carrier frequency and output pulse height (screw driver adjustments) made four of these units operate normally, but one unit (TT6-175) would not respond satisfactorily after attempted adjustment.

The method for testing the eight transponders for frequency drift versus temperature change was as follows: The transponder was placed in the Delta temperature test chamber; with the transponder energized and triggered, the temperature was controlled alternately to 100°F, 75°F, 50°F, 25°F, -20°F, and -40°F in 5-min steps; at each 5-min interval and at a discreet temperature setting, drift in carrier frequency was recorded from the spectrum analyzer L-20 as per controlled temperature change.

The tests showed a difference in radio frequency pulse amplitudes, which is a very good indication of expected tracking radar range, since this distance is a direct function of the inverse square law. This is true, of course, if one does not consider the atmospheric propagation properties at the time of transponder flight.

Because adequate sensitive field strength meters were not available to this office at the time of this report, no absolute values of transponder wattage outputs were recorded. Instead, relative measurements were made. A transponder (S# TT6-290) was selected which indicated an r-f pulse with maximum amplitude as compared to the balance of this lot. It was assumed that the power output exceeded 1.5 W. Using this unit as a reference, the pulse amplitude of the remaining transponders was monitored and the difference logged in decibels.

Since all workable transponders were successfully received by the radar during the 26-m distance check, it is difficult to quantitatively correlate the r-f pulse amplitude of the transponders with an expected radar range.

In addition to the Cordin Company solid state transponders, two similar units by another manufacturer were tested for comparison. Unit one had a bandwidth of 5.0 MHz at the main side lobe peak that was at the 10-dB down level. The sensitivity measured -19.5 dB and the detected output pulse indicated a 0.4-μs width at -0.90-V amplitude. Unit two measured 4.5-MHz bandwidth at the 10-dB down level, which corresponded to the first side lobe peak. The sensitivity and detected output pulse measured -18.4 dB and 0.6 μs at -1.20 V respectively. The results of these tests showed that the bandwidth on each unit is wider than that of any of the working models made by the Cordin Company.

In conclusion, although the spectrum analyzer indicated a wide variation in r-f pulse amplitude, radar-received transponder signals were not affected at a 26-m range. We believe that these solid state transponders almost without exception, could be tracked to the maximum range of our radar. A transponder output pulse width of between 0.8 and 2.2 μs does not affect the performance of the unit, and the radar will automatically lock on these transponders.

The wide variation of transponder sensitivities did not hamper the signal received 26 m from the radar. We do not believe that ransponder sensitivity is any problem for M-33 radar-transponder tracking since the X-band radar power level can be controlled for optimum transponder performance. This is especially true for radar automatic tracking mode.

2.4 Radar-Tetroon Aerial Monitoring

During the last 6 months, a feasibility study was conducted with tetroons, transponders, and aircraft in the location of radioactive plumes and ground contamination. The study consisted of locating an M-33 radar at East Butte and installing commercial power. The plan was to have a tetroon-transponder release automatically from a reactor area, then dispatch a radar crew to East Butte, locate the tetroon-transponder system and follow it while waiting for a monitoring aircraft with telemetering radio to become airborne. The aircraft, which also had ESSA transponders attached to it, was located by searching procedures and directed to the contaminant in the vicinity of the previously located tetroon. With the radar following the aircraft and the telemetry reporting to digitized radar, the x, y, z location of the aircraft and the radiation values at each position were known. Sine readings were taken once every second, the resolution of the aircraft flying at 110-120 mph was approximately every 200 ft. This information was stored on magnetic tape and processed by the computer, in which the data were isoplethed according to radiation values at different heights. A plot of the exact area flown

was also made. The aircraft has the capability of monitoring and telemetering ground contamination. For example, after one Controlled Environmental Radioiodine Test, the aircraft flew over the area 2 days after the material had been deposited. Figure 30 illustrates the resolution of radiation readings. These data were also compared with samples taken from pasture area and calibrations were accomplished. Further research is being conducted in calculating and flying tetroons at predetermined height levels since these inflated balloons are sometimes stored for months at a time.

2.5 Diffusion and Deposition Comparison Studies

For many years, atmospheric diffusion has been measured at the NRTS through field releases of uranine dye. The resulting climatology of atmospheric diffusion has been routinely used for calculations of diffusion of radioactive pollutants, such as molecular iodine. Does the application of a diffusion climatology derived from uranine dye effluent studies yield accurate estimates of the diffusion of molecular iodine?

To answer this question, field releases of uranine dye and molecular iodine were made to directly compare the diffusion of each tracer. The first field experiment, CDT I, was a continuous, 30-min, simultaneous release of molecular iodine and uranine dye during November 1967. It suggested that vertical diffusion or deposition was distinctly different for these two materials. Accepting these results, what physical process occurred to cause the vertical flux difference? Is this phenomenon dependent or influenced by the presence of particulates, such as uranine dye, in the atmosphere in excess of some minimum concentration? Also, what can be said about the deposition of uranine dye in an absolute sense?

To answer most of these questions a two-part field experiment (CDT II and CDT III) was conducted. Each of these tests was to be a 30-min, continuous release of effluents sampled by Maypack-loaded Staplex high-volume air samplers. CDT II was a simultaneous release of uranine dye and methyl iodide (CH_3I). CDT III was a simultaneous release of molecular iodine and methyl iodide. Through use of the third effluent both uranine dye and molecular iodine were compared to methyl iodide, the nondepositing, inert tracer. By use of ratios of dye and molecular iodine to CH_3I, the effects of different atmospheric diffusion rates were normalized to permit a comparison of dye and molecular iodine again as in CDT I.

No comparison of molecular iodine tracer releases are planned at present. The release techniques and filter collection efficiencies are being examined by Idaho Nuclear Corporation chemists, and until their findings are known it is unwise to interpret the molecular iodine diffusion and deposition measurements. The reason for delaying the final analysis and comparison is suspected changes in filter collection efficiency with increased loading of molecular iodine in both the Hurlburt X-9344 glass fiber-type filter and the silver-impregnated Gelman E filter. No significant change in collection efficiency is anticipated for the MSA iodine-impregnated carbon cartridge.

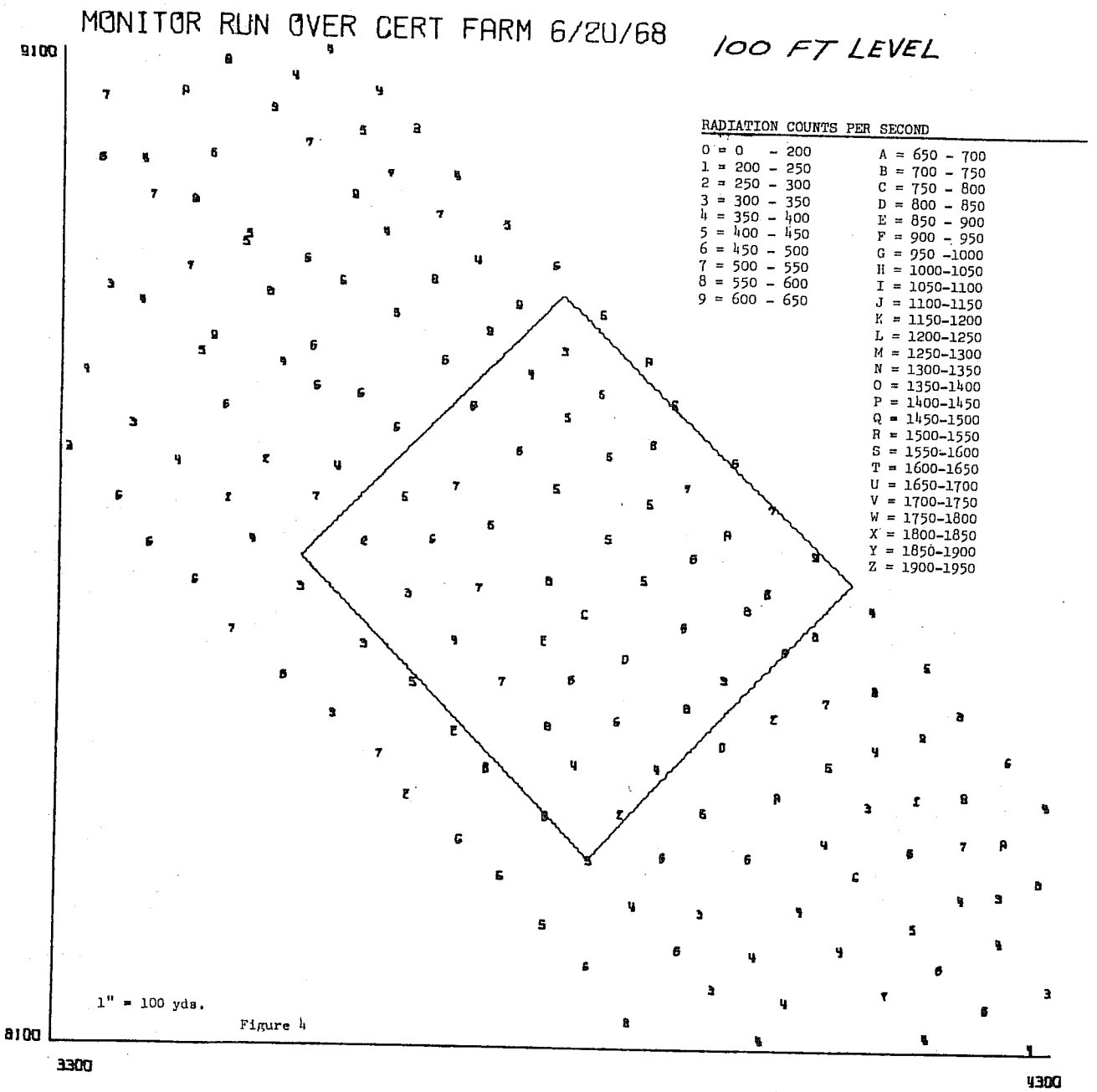

Figure 30. CERT Grid.

The summary presented below covers only the comparison of deposition and diffusion for uranine dye and methyl iodine, since their sampling is unaffected by the suspected variations in collection efficiencies.

The CDT II field test was conducted from 1006 to 1041 MST on May 7, 1968, at the Grid III diffusion site. The meteorological observations of winds and temperatures are summarized in table 7. The sky was partly cloudy, with a broken layer of cumulus clouds based near the height of the mountain tops. The ground was dry.

Table 7. Meteorological Conditions During CDT II

Height (m)	1	2	4	8	16	32	61
Wind Speed (mph)	7.0	-	8.4	8.6	9.4	-	10.9
Wind Direction (deg)	-	-	244	-	238	-	243
Temperature (^{o}F)	-	50*	-	-	-	-	45

* Temperature measured at 5 ft.

The diffusion measurements, from samples collected 1 m above the ground, are summarized in table 8 through a listing by arcs of the standard deviation, σ_y, of the lateral effluent mass distributions and by a wind speed and source strength normalized crosswind integrated concentration, $C\bar{u}/Q$. The general atmospheric diffusion conditions were between classes A and B. The diffusion observed in CDT II agreed with the climatologically expected diffusion on Grid III.

Table 8. Diffusion Measurements vs. Distance During CDT II

	Arc (m)				
	100	200	400	800	1600
DYE: σ_y (m)	24	43	75	163	258
CH_3I: σ_y (m)	29	45	78	177	396
DYE: $C\bar{u}/Q$ (m^{-1})x10^{-3}	33.5	12.0	3.0	1.2	0.5
CH_3I: $C\bar{u}/Q$ (m^{-1})x10^{-3}	94.6	44.2	11.3	4.4	1.8

Table 9 lists the ratios of wind-speed and source-strength normalized values of CIC by sampling arc. These ratios are proportional to the effect-

ive values of σ_z, the standard eviation of vertical effluent mass distribution. Both deposition and vertical diffusion effects are included in these ratios proportional to the effective σ_z.

Table 9. Ratios of CIC$\bar{u}$/Q (Methyl Iodide/Dye) vs. Distance During CDT II

ARC (m)	100	200	400	800	1600
Ratio	2.8	3.7	3.8	3.7	3.6

The CDT II comparison of uranine dye and methyl iodide yielded the following observations:

a) The lateral spreading of methyl iodide on all arcs was consistently about 10 percent greater than the lateral spreading of uranine dye.

b) Based on samples collected at 1-m heights, the crosswind integrated ($\chi\bar{u}$/Q) values for methyl iodide were about 3.5 times greater than the crosswind integrated ($\chi\bar{u}$/Q) values for uranine dye.

Since, for all practical purposes, methyl iodide is an inert, non-depositing gas any differences in combined vertical diffusion and surface deposition observed between uranine dye and methyl iodide must be a good estimate of the behavior of uranine dye in an absolute sense.

Air concentrations of uranine dye and methyl iodide were measured by high volume air samplers positioned on four 100-ft towers located near the 400-m sampling arc. The tower sampler data are summarized in table 10. The sum of all tower sampled values of $\chi\bar{u}$/Q for each tracer is proportional to the downwind flux of effluent through a vertical plane normal to the plume axis. The ratio of the downwind flux of methyl iodide to the downwind flux of uranine dye is three, within plus or minus 10 percent, which is comparable to the vertical flux ratio for transport away from the horizontal plane (as listed in table 9). When we recall the 10 percent uncertainty in the diffusion calculations, the differences in ratio at the various tower levels is significant only to the extent that they show the ratio to be larger near the ground and smaller near the tower tops. This deposition factor of three means that about 66 percent of the uranine dye released was deposited between the release point and 400 m downwind. This plume depletion result agrees with the Grid III deposition measurements reported by Islitzer and Dumbauld (1963).

In conclusion, the diffusion of uranine dye is representative of the lateral diffusion of an aerosol, such as methyl iodide. Uranine dye deposits readily during the first few hundred meters of travel, so that concentrations of inert, nondepositing aerosols are underestimated by a factor of about three during diffusion under strong temperature lapse conditions. These conclusions are based on the results of a single field release of uranine dye and methyl iodide. But in view of their agreement with the findings of

Table 10. Tower Values of $(\chi\bar{u}/Q)^*$ for 400 Meters Downwind

	Sampling Height (m)												Dye	Methyl	
	SFC		20'		40'		60'		80'		100'				
Tower	D	M	D	M	D	M	D	M	D	M	D	M	$\overline{\sum(\chi\bar{u}/Q)}$ (1)	$\overline{\sum(\chi\bar{u}/Q)_M}$ (2)	$(\sum)_M/(\sum)_D$
1	.67	1.8	.52	2.0	.68	1.3	.52	1.0	.39	2.2	.51	1.2	.55	1.58	2.9
2	.93	3.1	.85	1.7	1.1	2.5	1.0	2.5	1.0	2.6	.79	2.0	.95	2.40	2.5
3	2.0	5.2	2.0	5.2	1.8	6.5	1.4	5.4	1.6	3.8	1.4	3.8	1.7	4.98	2.9
4	1.8	5.9	(1.8)	(6.0)	1.7	6.4	1.4	5.1	2.1	(4.4)	1.7	4.3	(1.75)	(5.35)	(3.1)
Average	1.4	4.0	(1.3)	(3.7)	1.3	4.2	1.1	3.5	1.3	(3.3)	1.1	2.8	SUM 4.95	14.31	-
Ratio	3.0		(2.8)		3.2		3.2		(2.6)		2.6		Ratio of sums (2)÷(1)=2.9		

*All $\chi\bar{u}/Q$ values x 10^{-2} with units (m^{-2})

$(\sum)$ denotes estimated values of $\chi\bar{u}/Q$

D denotes measured values for uranine dye

M denotes measured values for methyl iodide

many previous studies of diffusion or deposition at the same location, the results of this single test are more meaningful.

Similar comparisons will be made for molecular iodine/methyl iodide and molecular iodine/uranine dye after the study of molecular release techniques and filter collection efficiences has been completed.

2.6 An Objective Forecast Technique Combining Map Types and Regression Estimation of Event Probabilities

Of the two general approaches to objective forecast development in meteorology, statistical and numerical-dynamical, the former is most easily developed and utilized at a field forecast office, and current forecast research follows the statistical approach for this reason. The purpose here is to investigate the use of objectively derived map types as predictors in the general statistical model REEP (regression estimation of event probabilities) and apply this model to forecasting precipitation at the NRTS. Map types would seem to define the general circulation pattern in one comprehensive predictor, allowing more reduction of predictand variance with fewer selected predictors.

2.6.1 Map Types

Synoptic meteorology map types are, in the traditional sense, flow patterns defined by a single variable, e.g., sea level pressures or heights from a given constant pressure surface. Map types may be derived objectively as suggested by Lund (1963). The rules for objective map type derivation were:

1) Correlate the data points of each map to every other map in the sample.

2) Count the number of significant correlations to each map-arbitrarily taken to be 0.80 in this study.

3) Designate the map having the largest number of significant correlations as map type A, and remove all maps significantly correlated to type A from the sample.

4) From the remaining sample find the map having the largest number of other maps significantly correlated to it and designate it as map type B.

5) Remove all maps significantly correlated to type B from the sample and from the ever-decreasing sample select types C, D, etc, in exactly the same way until no more types can be found with a sufficient number of other maps significantly correlated to it--six in this study.

The object of using map types as predictors in REEP is to reduce the number of predictors needed to explain a certain amount of predictand variance. However, the use of more than one variable in the typing may

increase the predictive power in the same number of derived map types. These multivariable map types would be very difficult to distinguish subjectively in routine practice, however multivariable types were derived assuming routine objective determination is feasible.

Five map type schemes were developed as follows:

1) 500-mb heights taken from the 23 data points shown in figure 31a.

2) 500-mb heights from the same 23 data points plus 7 derived vorticities taken from the data points shown in figure 31b.

3) Same as the second experiment except that the vorticity data points were weighted so as to make vorticity have equal weight with the 500-mb heights.

4) 500-mb heights from the same 23 points plus 850-mb heights from the 10 points shown in figure 31c, where the crosses indicate weighted 850-mb heights were used.

5) 500-mb heights from the same 23 points plus derived weighted vorticities from the same 7 points, plus 850-mb heights from the same 10 points with the same 3 points weighted.

National Meteorological Center grid point tapes were used for input; the time for all data was 1200 GMT. The samples were taken from the months of April and May for the years 1962 through 1967. Due to missing maps 331 samples were used in the correlation analysis for schemes one, two, and three, and 319 for schemes four and five.

After the map types had been selected, the climatology sample belonging to each type was determined as consisting of every map from the original sample that was significantly correlated to the type map. Table 11 shows the number of maps significantly correlated to each type map for each scheme, the observed frequency of precipitation for the sample, and the number of individual maps significantly correlated to zero, one, two, three, four, five, or six map types. The forecasting ability of map types alone, derived from table 11, is presented later in tables 12 and 13 for comparison with forecasts from REEP equations.

2.6.2 The REEP Method and Experiments

A description of the REEP procedure is given by Miller (1964), and only the essential features are repeated here for a general understanding. The first characteristic is that all input variables, predictors, and predictands, are binary, or 0-1 variables. The second feature is its application to a predictand that may consist of a number of distinct groups. In the case of precipitation probability forecasting only one predictand exists since precipitation is a natural binary or yes-no variable. The third feature is that the derived prediction equations yield probability estimates for each predictand group, there being one equation for each group.

a. b. c.

Figure 31. Location of NMC grid points used in map type experiments: a) 23 points from which 500-mb data were taken, b) 7 points at which vorticity values were derived, and c) 10 points from which 850-mb data was taken.

Table 11. Number of Maps Significantly Correlated to the Type Maps from each of Five Experiments, and Observed Frequency of Precipitation for the Sample. One-Type Maps are Maps Significantly Correlated to Exactly One-Map Type, and Similarly for Two-Type, Three-Type, etc.

Experiment No.	1		2		3		4		5	
Type										
A	154	.17	103	.10	97	.08	92	.18	167	.15
B	105	.24	75	.19	62	.08	59	.03	116	.25
C	82	.12	56	.07	61	.07	57	.16	55	.04
D	67	.32	49	.10	54	.19	46	.30	54	.11
E	63	.43	42	.07	44	.07	44	.43	54	.35
F	36	.28	42	.19	30	.50	42	.05	44	.25
G	32	.25	31	.39	26	.04	39	.21	33	.42
H	29	.38	28	.29	22	.36	36	.31	33	.00
I	24	.17	28	.21	21	.29	32	.31	20	.35
J	23	.22	25	.36	16	.19	31	.10	16	.63
K	22	.27	23	.57	16	.12	28	.14	14	.29
L	21	.24	20	.25	15	.53	20	.15	13	.54
M	16	.38	19	.16	13	.31	17	.47	13	.62
N	16	.56	17	.18	12	.25	17	.35	12	.25
O	16	.50	12	.08	12	.50	16	.69	10	.50
P	7	.43	12	.42	12	.33	15	.00	6	.00
Q	7	.00	12	.25	11	.46	11	.18	6	.33
R	6	.17	11	.46	11	.18	11	.46	6	.50
S	6	.67	10	.40	11	.27	10	.00	6	.00
T			9	.44	10	.30	9	.67		
U			9	.22	10	.10	8	.12		
V			8	.25	9	.67	8	.75		
W			8	.25	9	.11	8	.00		
X			8	.63	8	.13	7	.00		
Y			7	.28	7	.42	7	.43		
Z			7	.28	7	.57	6	.33		

One-type maps	57	82	100	69	67
Two-type maps	98	74	83	63	108
Three type maps	88	69	57	63	90
Four-type maps	45	43	20	50	29
Five-type maps	7	10	13	16	2
Six-type maps	0	2	4	2	0
Untyped maps	36	51	54	56	23

The computational procedure is that of multiple regression where the set of predictors is the same for each of a number of regression equations which are derived simultaneously by a computational alogrithm upon the variance-covariance matrix of binary predictors. The computational procedure also allows for screening the predictors for those which yield the greatest reduction in variance after the effect of all previously selected predictors has been removed. The next selected variable is the one giving a greater reduction of variance in any one predictand group than any other variable will give for any one predictand group.

The description of variables in binary form was generalized into an option of three distinct methods in the model used for the experiments of this study. The first method, or option, called the "simple binary variable", applies to natural binary variables and continuous variables. Examples of natural binary variables are "the occurrence of measurable precipitation-- yes - coded 1 or no - coded 0", and "the occurrence of map type X- yes or no". A continuous variable, such as temperature, is made into 'n' simple binary variables by arbitrarily dividing the temperature scale into 'n' discrete groups. For any given observation one of these groups is "1" and the "n-1" remaining groups are "0". The second method, or option, called the "cumulative binary variable", applies to continuous predictors. It will often be of predictive advantage to use a predictor which is "yes" if it equals or exceeds a certain value, and "no" only for lower valued classes. Relative humidity may be advantageously used in this way by dividing the scale of 0 to 100 percent into 'n' arbitrary classes and assigning the coded value "one" to the class containing the value of the given observation and the coded value "one" to all higher valued classes. The coded value of "zero" is assigned to all lower valued classes. Another description of such a variable is "at least", for if in a given observation the coded value "one" occurs in a given class of interest, the information is that the observation was of "at least" this value. The third option is the creation of new natural binary predictors by the Boolean algebra of combining already derived binary predictors through the 'AND' and "OR' operations. For example, if a predictor is desired which says the relative humidity exceeds 80 percent and the 500-mb winds are in the SW quadrant, the cumulative predictor for relative humidity having a lower boundary of 80 percent is combined with the simple predictor for 500-mb winds in the SW quadrant. If both of the original predictors are coded "one" and the AND operation will yield the value "one" for the new Boolean predictor. If either or both of the original predictors had been coded "zero" the AND operation would have yielded the value "zero" for the new Boolean predictor. The OR operation requires both original predictors to be coded "zero" to get "zero" for the new Boolean predictor, and if either of the original predictors is coded "one" the new Boolean predictor is coded "one". Complex Boolean predictors may be derived by continuing to combine previously derived simple, cumulative or Boolean predictors by AND and OR operations to derive new Boolean predictors.

To test the relative effect when map type predictors in REEP are used, three equations were derived as follows:

1) Straight - meaning no map type predictors were used.

2) 500-mb - meaning 500-mb map types as derived in map type scheme one were included among the predictors.

3) 500-mb plus vorticity - meaning 500-mb plus vorticity map types as derived in map type scheme two were included among the predictors.

In the first REEP experiment the Boolean predictors were chosen so as to partially classify the type of circulation to see if the results would compare favorably when map types were used in experiments two and three. In the second and third experiments the Boolean predictors were chosen to combine dry and wet map types and combine the combinations of types with various humidity predictors. The selection of predictors was limited by a program capacity of 125 binary predictors and predictands.

The REEP experiments were run on a 5-year data sample, April and May for 1962 through 1966. Data were not available for 1967 to completely overlap the map type sample. The sample sizes were 303 for the first experiment, which had 2 days missing data, and 268 for the second and third experiments, which had an additional 35 missing days due to missing maps in the map-typing sample.

2.6.3 Forecast Comparison Results

Table 12 shows the significance of Brier score evaluation of the forecasts made by each of the eight experiments. The formulas to compute μ, the climatological Brier score; $\bar{P}$, the Brier score of the predictions; S_o, the sample standard deviation; and 't', the Student's 't', are:

$$\mu = \frac{1}{N} \sum \left(O_i - \frac{\Sigma O_i}{N} \right)^2 ,$$

$$\bar{P} = \frac{1}{N} \sum (O_i - P_i)^2 ,$$

$$S_o = \left(\frac{\Sigma O_i - (\Sigma O_i)^2 / N}{N} \right)^{1/2} , \text{ and}$$

$$t = \frac{(\mu - \bar{P})\ (N - 1)^{1/2}}{S_o} ,$$

where N is the sample size, O_i is the observed probability of the i^{th} observation, and P_i is the predicted probability of the i^{th} observation.

In the $\bar{P}$ computations for map types, a sample whose size was equal to the sum of map type samples was used, namely, the summation of the first column for each experiment in table 11, which is equivalent to averaging the predicted probabilities from all the types to which a given day is significantly correlated.

Table 12. Statistical Significance Comparison of the Map Type and REEP Precipitation Forecasts

	Map Type Experiments					REEP Experiments		
	1	2	3	4	5	1	2	3
N	331	331	331	319	319	303	268	268
ΣO_i	80	80	80	76	76	77	67	67
S_o	.428	.428	.428	.426	.426	.435	.433	.433
μ	.183	.183	.183	.182	.182	.190	.188	.188
$\bar{P}$	.179	.147	.132	.146	.153	.150	.102	.099
t	.278	2.179	2.931	2.197	1.770	1.595	3.251	3.365

Probability of larger t, sign considered

	$t_{.10}$	$t_{.05}$	$t_{.01}$	$t_{.0005}$
Tabled t's	1.28	1.65	2.34	3.33

The Student's - t test for the significance of the term, $\mu - \overline{P}$, shows that except for 500-mb map types (map type experiment one), each of the map type experiments resulted in a significant improvement over climatology. Reference to table 13 shows that the problem with the first map type experiment is a lack of sharpness (i.e., forecasts of very high and very low probabilities), as most of the types in experiment one predicted precipitation probabilities not much different from climatology. There was considerable increase in sharpness for low probabilities in map type experiments two, three, four, and five, which accounts for the lower Brier scores of these experiments. The conclusion may be drawn that multiparameter map types discriminate precipitation probabilities better than simple map types, namely 500-mb types. Intuition would lead one to expect the most sophisticated experiment, number five, to give the greatest improvement. The reason that this experiment gave the poorest results of the multiparameter types probably lies in the number of data points used per map. With 40 data points, a perturbation may be distributed over a larger number of points, without significant change in the correlation between two otherwise identical maps compared with the correlation obtained when the number of data points per map are 23, 30, or 33, as in the first four experiments. Consequently, major changes are possible in the ten 850-mb data points of three variable (40 point) map types and still maintain significant correlation to other maps similar in 500-mb pattern only. A careful designing of the number of data points and their weighting relative to the size of disturbances to be allowed in the map types would very likely change the order of significance of the five map type experiments. A later experiment based on 23 500-mb data points, 7 weighted vorticity points, and 10 weighted points of the thickness between the 1000-mb and 500-mb layers, all points more centered around SE Idaho than in the five experiments already described, yielded a $\overline{P}$ score of .133, which is comparable with the best of the five experiments described here.

The Student's - t test applied to the improvement of REEP over climatological Brier scores showed significance at the 5 percent level of confidence when no map types were used, and significance at the .05 percent level of confidence when map types were used. There was no significant difference in the results when 500-mb plus vorticity types were used as opposed to 500-mb types. Of the total reduction of variance in equation one, 15 percent was due to Boolean predictors characterizing the flow pattern; consequently, the improvement of the REEP equations with map types over the equation without map types would have been even greater if no characterization of the flow with Boolean predictors had been attempted.

In the Brier score results, the map type experiment involving 500-mb height and weighted vorticity compares quite favorably with REEP experiments two and three. This result is misleading, since table 13 shows that forecasts purely from map types have a distinct lack of precipitation forecasts, i.e., probabilities of 50 percent or greater. Therefore, the prefigurance (Panofsky and Brier, 1958) percentage, the percentage of events correctly forecast, is quite poor for all the map type experiments. Postagreement, the percentage of forecasts that were verified, was fairly high for all eight experiments simply because a no-rain forecast in a dry area has a high probability of being verified, and nearly all map type forecasts were for no

Table 13. Number of Cases of Forecast Probabilities, Observed Precipitation Classes, and Prefigurance and Postagreement Ratios

	<10	10-20	20-30	30-40	40-50	50-60	60-70	70-80	80-90	>90	Total Cases
Map Type Experiment 1											
Forecast	4	85	121	57	22	1	5	0	0	0	295
Observed	0	9	25	22	13	1	3	0	0	0	73
	Prefigurance .52			Postagreement .71							
Map Type Experiment 2											
Forecast	54	109	51	33	24	7	2	0	0	0	280
Observed	4	16	14	12	10	6	2	0	0	0	64
	Prefigurance .54			Postagreement .85							
Map Type Experiment 3											
Forecast	91	66	34	36	39	9	2	0	0	0	277
Observed	5	11	10	11	20	6	2	0	0	0	65
	Prefigurance .54			Postagreement .76							
Map Type Experiment 4											
Forecast	47	79	48	46	23	8	11	1	0	0	263
Observed	0	10	11	18	8	7	9	1	0	0	64
	Prefigurance .63			Postagreement .83							
Map Type Experiment 5											
Forecast	62	83	69	45	14	11	12	0	0	0	296
Observed	0	14	20	18	7	8	6	0	0	0	73
	Prefigurance .59			Postagreement .70							
REEP Experiment 1											
Forecast	102	47	44	34	22	21	11	13	4	5	303
Observed	0	5	9	8	14	11	10	11	4	5	77
	Prefigurance .74			Postagreement .81							
REEP Experiment 2											
Forecast	103	32	36	32	19	15	16	6	5	4	268
Observed	2	2	9	10	9	9	13	4	5	4	67
	Prefigurance .74			Postagreement .81							
REEP Experiment 3											
Forecast	95	37	44	31	21	13	10	7	3	7	268
Observed	1	4	9	8	12	10	9	5	2	7	67
	Prefigurance .74			Postagreement .84							

rain. The relatively poor postagreement of map type experiment five is largely due to the poor verification of the precipitation forecasts that were made; only 14 of 23 were correct.

In summary, the Brier score evaluations showed multivariable map types to be more effective than single variable map types in predicting precipitation by map types alone, however there was little difference in the map typing scheme used when applied as predictors in REEP. The map typing schemes in REEP made improvement over the REEP equation without map types. In addition, the Brier scores for forecasts made by map types alone were nearly as good as forecasts made by REEP equations with map type predictors. Another test, the prefigurance score, the percentage of cases correctly forecast, showed much better results with all the REEP equations when compared to the prefigurance scores for any of the map-type-alone forecasts. The prefigurance weakness of the map-type-alone forecasts, along with the Brier score weakness of REEP without map type predictors shows the REEP with map type predictors equations to be significantly superior to all other schemes attempted with only slight advantage in all tests to the REEP with multivariable map types.

The use of map type predictors in REEP should result in a significant reduction of variance if the predictand is physically dependent upon the synoptic scale flow pattern. The greater the dependence of the predictand upon the synoptic scale flow pattern, as opposed to dependence upon other predictors, the greater is the significance of the reduction of variance when map type predictors are used. This dependence is often a function of the time scale of the predictand, as in the case of precipitation. The reduction of variance in precipitation forecasting for periods of 12 hr and less should be much greater when humidity, wind direction, and wind shear predictors are used; however, if the forecast period is 24 to 36 hr the map type predictors should result in far more reduction of variance than current observations of humidity, wind direction, and wind shear. This became evident when an operational REEP equation for April and May was derived from a set of predictors consisting of the 500-mb map types from map type experiment one, 500-mb heights; 500-mb gradients; 500-mb geostrophic wind direction; and Boolean combinations of these. These predictors may all be selected from prognostic charts. On the TODAY period of the forecast the subjective forecasts for April and May 1968 had a Brier score verification of .101 while the operational REEP had a Brier score of .148. On the TOMORROW period of the forecast the operational REEP had a Brier score of .158 while the forecaster jumped to .188. The REEP was verified from the prognostic charts on the TOMORROW period to be in fair competition with the forecaster.

3.0 REFERENCES

Angell, J. K. (1962), "On the use of tetroons for the estimation of atmospheric dispersion on the mesoscale," Monthly Weather Rev. 90, No. 7, 263-270.

Angell, J. K., D. H. Pack, and C. R. Dickson (1968), "A Lagrangian study helical circulations in the planetary boundary layer," J. Atmospheric Sci. 25, No. 5, 707-717.

Bingham, C., M. D. Godfrey, and J. W. Tukey (1967), "Modern techniques of power spectrum estimation," IEEE Trans. Audio Electroacoustics AU-15, No. 2, 56-66.

Blackman, R. B. and J. W. Tukey (1958), The Measurement of Power Spectra (Dover Publications, N. Y.), 190 pp.

Cooley, J. W. and J. W. Tukey (1965), "An algorithm for the machine calculation of complex Fourier series," Math. Comp. 19, No. 90, 297-301.

de Jong, H. M. (1958), "Errors in upper-level wind computations," J. Meteorol. 15, No. 2, 131-137.

Dickson, C. R., G. E. Start, E. H. Markee, Jr., A. P. Richter, and J. Kearns (1967), "Meteorology for the loss of fluid test reactor," Progress Report, January 1966-January 1967, U. S. Atomic Energy Commission Technical Report IDO-12059, 55 pp.

Giblett, M. A. (1932), "The structure of wind over level country," Geophysical Memoirs No. 54, Met. Off. Air Ministry, Great Britian, 119 pp.

Hilsmeier, W. F. and F. A. Gifford (1962), "Graphs for estimating atmospheric dispersion," U. S. Atomic Energy Commission Technical Report, ORO-545, 10 pp.

Islitzer, N. F. and R. K. Dumbauld (1963), "Atmospheric diffusion-deposition studies over flat terrain. Int. J. Air Water Pollution 7, 999-1022.

Kao, S. K. and L. Wendell (1968), "Some characteristics of relative particle dispersion in the atmospheric boundary layer." Atmospheric Environ. 2, No. 3, 397-407.

Laby, J. E. and J. G. Sparrow (1965), "Wind studies using level balloons," J. Appl. Meteorol. 4, No. 5, 585-589.

Lund, I. A. (1963), "Map pattern classification by statistical methods," J. Appl. Meteorol. 2, No. 1, 56-65.

Miller, R. G. (1964), "Regression estimation of event probabilities," Travelers Research Center Report No. 7411-121, Weather Bureau Contract 10704, 153 pp.

Ohnsorg, F. (1957), "Error estimates for constant-level balloon tracking," J. Meteorol. 14, No. 1, 51-83.

Panofsky, H. A. and G. W. Brier (1958), Some Applications of Statistics to Meteorology (Penn State Univ., Mineral Industries Extension Services), 224 pp.

Smith, M. E. (1950), "The forecasting of micrometeorological variables," AECU-702, U. S. Atomic Energy Commission Technical Information Division, Oak Ridge, Tenn., 10 pp.

4.0 REVIEW OF REACTOR SAFETY ANALYSIS REPORTS

The Air Resources Laboratory in Silver Spring, Maryland, and the Field Office in Idaho have continued to take an active part in the review of reactor safety analysis reports as well as consultations with regard to the preparation of the reports. In addition, written comments have been prepared for the Division of Reactor Licensing through the Division of Reactor Development and Technology as follows:

1. Rancho Seco Nuclear Generating Station Unit No. 1, Sacramento Municipal Utility District Preliminary Safety Analysis Report, Volumes I, II, III, and IV, dated November 1967.

2. Russellville Nuclear Unit, Arkansas Power and Light Company Preliminary Safety Analysis Report, Volumes I and II, dated November 29, 1967.

3. Donald C. Cook Nuclear Plant, Indiana and Michigan Electric Company Preliminary Safety Analysis Report, Volumes I, II, and III, dated December 18, 1967.

4. Pilgrim Nuclear Power Station, Boston Edison Company Design and Analysis, Amendment 4, dated December 28, 1967.

5. Salem Nuclear Generating Station (formerly Burlington Nuclear Generating Station), Public Service Electric and Gas Company Preliminary Facility Description and Safety Analysis Report, Volumes I, II, III, and IV, dated January 22, 1968.

6. Calvert Cliffs Nuclear Power Plant Units 1 and 2, Baltimore Gas and Electric Company Preliminary Safety Analysis Report, Volumes I and II, dated January 1968.

7. Ginna (formerly Brookwood) Nuclear Power Plant, Unit No. 1, Rochester Gas and Electric Corporation Final Facility Description and Safety Analysis Report, Volumes 1 and 2, dated January 24, 1968.

8. Surrey Power Station, Units No. 1 and 2, Virginia Electric and Power Company Preliminary Safety Analysis Report, Amendment No. 3, dated August 24, 1967.

9. Fort Calhoun Station, Unit No. 1, Omaha Public Power District Facility Description and Safety Analysis Report, Supplement No. 3, dated September 25, 1967, Supplement No. 5, dated September 29, 1967, and Question raised by Licensing Board.

10. Millstone Nuclear Power Station, Unit No. 1, Final Safety Analysis Report, Volumes I, II, and III, dated March 15, 1968.

11. Indian Point Nuclear Generating Unit No. 3, Consolidated Edison Company of New York, Inc. Preliminary Safety Analysis Report, Exhibit B, Volumes 1, II, and II, Part B, dated April 1968.

12. Oyster Creek Nuclear Station, Unit No. 2, Jersey Central Power and Light Company Preliminary Safety Analysis Report, Volumes I, II, and III, dated April 29, 1968.

13. Rancho Seco Nuclear Generating Station, Unit No. 1, Sacramento Municipal Utility District Preliminary Safety Analysis Report, Amendment No. 2, dated April 12, 1968.

14. Bell Station, New York State Electric and Gas Corporation Preliminary Safety Analysis Report, Volumes I, II, and III, dated March 25, 1968.

15. Donald C. Cook Nuclear Plant, Indiana and Michigan Electric Company Preliminary Safety Analysis Report, Amendment No. 2, dated June 6, 1968.

5.0 PUBLICATIONS

1. Angell, J. K., D. H. Pack, W. A. Hass, and W. H. Hoecker, "Tetroon flights over New York City," Weather 23, No. 5, 184-191, May 1968.

2. Hosler, C. R., "Urban-rural climatology of atmospheric radon concentrations," J. Geophys. Res. 73, No. 4, 1155-1166, February 1968.

3. Markee, E. H., Jr. (contributor), "Controlled environmental radioiodine tests," Progress Report No. 3 (Meteorological aspects of deposition), U. S. Atomic Energy Commission Report No. IDO-12063, 77 pp., January 1968.

6.0 LABORATORY PERSONNEL

Idaho Falls, Idaho

Duanna Walker, temporary clerk-typist, resigned April 5, 1968.

Judith R. Zavala, temporary clerk-stenographer enter on duty April 8, 1968.

Annette Barnes, temporary scientific assistant, entered on duty June 3, 1968.

David E. Johnson, electronic technician, resigned June 21, 1968.

William L. Wiser, temporary summer working aid, entered on duty June 24, 1968.